



Natural Resources
Canada

Ressources naturelles
Canada



Microstructure and Hardness Characterization of Girth Welds

Final Report 278-T-03

For Project

Development of Optimized Welding Solutions for X100 Line Pipe Steel

Prepared for the

Design, Materials, and Construction Technical Committee of
Pipeline Research Council International, Inc.
Project MATH-1 Catalog No. L5XXXX

and

U.S. Department of Transportation
Pipeline and Hazardous Materials Safety Administration
Office of Pipeline Safety
Agreement Number DTPH56-07-T-000005

Prepared by

J.A. Gianetto, G.R. Goodall and W.R. Tyson
CANMET Materials Technology Laboratory

M.A. Quintana and V.B. Rajan,
The Lincoln Electric Company

Y. Chen
Center for Reliable Energy Systems

September 2011

This research was funded in part under the Department of Transportation, Pipeline and Hazardous Materials Safety Administration's Pipeline Safety Research and Development Program. The views and conclusions contained in this document are those of the authors and should not be interpreted as representing the official policies, either expressed or implied, of the Pipeline and Hazardous Materials Safety Administration, or the U.S. Government.

CANMET Materials Technology Laboratory

Microstructure and Hardness Characterization of Girth Welds

J.A. Gianetto, G.R Goodall and W.R Tyson

CANMET Materials Technology Laboratory
Minerals and Metals Sector, Natural Resources Canada
183 Longwood Road South, Hamilton, ON, Canada, L8P 0A5

M.A. Quintana and V.B. Rajan,
The Lincoln Electric Company

Y. Chen
Center for Reliable Energy Systems

CANMET Report No. 2011-04(TR)

September 2011

Disclaimer

Natural Resources Canada makes no representations or warranties respecting the contents of this report, either expressed or implied, arising by law or otherwise, including but not limited to implied warranties or conditions of merchantability or fitness for a particular purpose.



Catalog No. L5XXXX

MICROSTRUCTURE AND HARDNESS CHARACTERIZATION OF GIRTH WELDS

Final Report 278-T-03

For Project

Development of Optimized Welding Solutions for X100 Line Pipe Steel

Prepared for the

Design, Materials, and Construction Technical Committee of
Pipeline Research Council International, Inc.
Project MATH-1 Catalog No. L5XXXX

and

U.S. Department of Transportation
Pipeline and Hazardous Materials Safety Administration
Office of Pipeline Safety
Agreement Number DTPH56-07-T-000005

Prepared by

J.A. Gianetto, G.R Goodall and W.R Tyson
CANMET Materials Technology Laboratory

M.A. Quintana and V.B. Rajan,
The Lincoln Electric Company

Y. Chen
Center for Reliable Energy Systems

September 2011

Version	Date of Last Revision	Date of Uploading	Comments
2	2 April 2011	4 April 2011	References to be inserted after review.
Final	1 September 2012	1 December 2011	Final Report

This report is furnished to Pipeline Research Council International, Inc. (PRCI) under the terms of PRCI contract [278-PR- 348 - 074513], between PRCI and the MATH-1 contractors:

- Electricore (prime contractor),
- Center for Reliable Energy Systems, CANMET, NIST, and The Lincoln Electric Company (sub-contractors).

The contents of this report are published as received from the MATH-1 contractor and subcontractors. The opinions, findings, and conclusions expressed in the report are those of the authors and not necessarily those of PRCI, its member companies, or their representatives. Publication and dissemination of this report by PRCI should not be considered an endorsement by PRCI of the MATH-1 contractor and subcontractors, or the accuracy or validity of any opinions, findings, or conclusions expressed herein.

In publishing this report, PRCI and the MATH-1 contractors make no warranty or representation, expressed or implied, with respect to the accuracy, completeness, usefulness, or fitness for purpose of the information contained herein, or that the use of any information, method, process, or apparatus disclosed in this report may not infringe on privately owned rights. PRCI and the MATH-1 contractors assume no liability with respect to the use of, or for damages resulting from the use of, any information, method, process, or apparatus disclosed in this report. By accepting the report and utilizing it, you agree to waive any and all claims you may have, resulting from your voluntary use of the report, against PRCI and the MATH-1 contractors.

Pipeline Research Council International Catalog No. L5XXXX

PRCI Reports are Published by Technical Toolboxes, Inc.

3801 Kirby Drive, Suite 520
Houston, Texas 77098
Tel: 713-630-0505
Fax: 713-630-0560
Email: info@ttoolboxes.com

PROJECT PARTICIPANTS

PROJECT TEAM MEMBER	COMPANY AFFILIATION	PROJECT TEAM MEMBER	COMPANY AFFILIATION
Arti Bhatia	Alliance	Jim Costain	GE
Jennifer Klementis	Alliance	Gilmar Batista	Petrobras
Roger Haycraft	Boardwalk	Marcy Saturno de Menezes	Petrobras
David Horsley	BP	Dave Aguiar	PG&E
Mark Hudson	BP	Ken Lorang	PRCI
Ron Shockley	Chevron	Maslat Al-Waranbi	Saudi Aramco
Sam Mishael	Chevron	Paul Lee	SoCalGas
David Wilson	ConocoPhillips	Alan Lambeth	Spectra
Satish Kulkarni	El Paso	Robert Turner	Stupp
Art Meyer	Enbridge	Gilles Richard	TAMSA
Bill Forbes	Enbridge	Noe Mota Solis	TAMSA
Scott Ironside	Enbridge	Philippe Darcis	TAMSA
Sean Keane	Enbridge	Dave Taylor	TransCanada
Laurie Collins	Evraz	Joe Zhou	TransCanada
David de Miranda	Gassco	Jason Skow	TransGas
Adriaan den Herder	Gasunie	Ernesto Cisneros	Tuberia Laguna
Jeff Stetson	GE	Vivek Kashyap	Welspun
		Chris Brown	Williams

CORE RESEARCH TEAM	
RESEARCHER	COMPANY AFFILIATION
Yaoshan Chen	Center for Reliable Energy Systems
Yong-Yi Wang	Center for Reliable Energy Systems
Ming Liu	Center for Reliable Energy Systems
Dave Fink	Lincoln Electric Company
Marie Quintana	Lincoln Electric Company
Vaidyanath Rajan	Lincoln Electric Company
Joe Daniel	Lincoln Electric Company
Radhika Panday	Lincoln Electric Company
James Gianetto	CANMET Materials Technology Laboratory
John Bowker	CANMET Materials Technology Laboratory
Bill Tyson	CANMET Materials Technology Laboratory
Guowu Shen	CANMET Materials Technology Laboratory
Dong Park	CANMET Materials Technology Laboratory
Timothy Weeks	National Institute of Standards and Technology
Mark Richards	National Institute of Standards and Technology
Dave McColskey	National Institute of Standards and Technology
Enrico Lucon	National Institute of Standards and Technology
John Hammond	Consultant Metallurgist & Welding Engineer

This Page Intentionally Left Blank

FINAL REPORT STRUCTURE

Focus Area 1 - Update of Weld Design, Testing, and Assessment Procedures for High Strength Pipelines		
Report #	Description	Lead Authors
277-T-01	Background of Linepipe Specifications	CRES/CANMET
277-T-02	Background of All-Weld Metal Tensile Test Protocol	CANMET/Lincoln
277-T-03	Development of Procedure for Low-Constraint Toughness Testing Using a Single-Specimen Technique	CANMET/CRES
277-T-04	Summary of Publications: Single-Edge Notched Tension SE(T) Tests	CANMET
277-T-05	Small Scale Tensile, Charpy V-Notch, and Fracture Toughness Tests	CANMET/NIST
277-T-06	Small Scale Low Constraint Fracture Toughness Test Results	CANMET/NIST
277-T-07	Small Scale Low Constraint Fracture Toughness Test Discussion and Analysis	CANMET/NIST
277-T-08	Summary of Mechanical Properties	CANMET
277-T-09	Curved Wide Plate Tests	NIST/CRES
277-T-10	Weld Strength Mismatch Requirements	CRES/CANMET
277-T-11	Curved Wide Plate Test Results and Transferability of Test Specimens	CRES/CANMET
277-S-01	Summary Report 277 Weld Design, Testing, and Assessment Procedures for High Strength Pipelines	CRES

Focus Area 2 - Development of Optimized Welding Solutions for X100 Linepipe Steel		
Report #	Description	Lead Authors
278-T-01	State of The Art Review	Lincoln
278-T-02	Material Selection, Welding and Weld Monitoring	Lincoln/CANMET
278-T-03	Microstructure and Hardness Characterization of Girth Welds	CANMET/Lincoln
278-T-04	Microstructure and Properties of Simulated Weld Metals	CANMET/Lincoln
278-T-05	Microstructure and Properties of Simulated Heat Affected Zones	CANMET/Lincoln
278-T-06	Essential Welding Variables	Lincoln/CANMET
278-T-07	Thermal Model for Welding Simulations	CRES/CANMET
278-T-08	Microstructure Model for Welding Simulations	CRES/CANMET
278-T-09	Application to Other Processes	Lincoln/CANMET
278-S-01	Summary Report 278 Development of Optimized Welding Solutions for X100 Line Pipe Steel	Lincoln

Executive Summary

Strain-based design for pipeline projects requires overmatching the strength of the weld metal (WM) relative to the parent pipe to avoid strain localization in the weldment during service. Achieving the required strength overmatch, ductility and low temperature toughness in WM becomes a challenge as the strength of the pipe increases. The introduction of higher productivity advanced pulsed gas metal arc welding (GMAW-P) processes adds further complications from the associated cooling conditions of the weldment. An improved understanding of WM systems (compositions, microstructures, essential variables, etc.) required for the successful large scale production of high strength pipeline field girth welds is needed for new and demanding pipeline construction projects.

In this study, the WM microstructures formed in single and dual torch GMAW-P X100 pipe welds were characterized using conventional metallographic methods and mapping of microhardness across the entire weld region. The results were compared with a single pipe composition and welding consumable in order to relate differences in microstructure to the welding conditions and weld pass sequence. The work on full pipe welds was supplemented by a series of staggered bead pipe welds and flat plate welds using the same pipe steel. The staggered bead pipe welds provided a systematic assessment of microstructure development with the deposition of successive weld beads. Plate welds, replicating the joint geometry used for the pipe welds and fabricated at both high and low cooling rates, revealed additional information about microstructure development relative to weld thermal cycle. Detailed assessment related to each deposited weld bead from the hot, fill, and cap passes has allowed the proportion of as-deposited (AD) and reheated (RH) weld metal to be quantified in terms of microstructure and microhardness.

Significant variation in the microstructural constituents was observed in both the weld metal (WM) and the heat affected zone (HAZ), particularly at the faster cooling rates typical of narrow gap GMAW-P pipeline girth welds. Microstructural changes occurred over very short distances, making assessment of potential influence on weld performance more difficult.

Table of Contents

Executive Summary	vii
Table of Contents	ix
List of Figures	x
List of Tables	xi
1 Introduction	1
2 Objective	1
3 Experimental Procedures	1
3.1 Materials	2
3.2 Baseline Single and Dual Torch Rolled Pipe Welds	2
3.3 Staggered Single and Dual Torch Rolled Pipe Welds	3
3.4 Single Torch Plate Weld	3
3.5 Metallography and Microhardness Traverses	3
3.6 Microhardness Measurement and Mapping	4
4 Results and Discussion	5
4.1 X100 Pipe Steel	5
4.2 Single And Dual Torch Rolled X100 Welds	6
4.3 Staggered Single and Dual Torch Rolled X100 Welds	8
4.4 Single Torch X100 Plate Welds	9
5 Summary and Conclusions	10
6 Acknowledgments	11
7 References	11

List of Figures

Figure 1. Single and dual torch roll welding.....	15
Figure 2. Schematic diagrams of joint geometry and pass sequences used for pipe welds.....	16
Figure 3. Representative macrographs of single and dual torch pipe welds. (Pipe wall thickness = 19 mm).....	16
Figure 4. Macrographs of staggered weld passes (a) single torch fill pass (F1) and (b) dual torch fill passes D1 and D2. X~2.5	17
Figure 5. Schematic of pass sequence (a) and macrograph of experimental plate weld (b).....	17
Figure 6. Macrograph of single torch X100 rolled pipe weld with vertical and horizontal lines indicating relative locations of through-thickness and cross-weld microhardness traverses. Enlarged image shows detail of through-thickness microhardness traverse in the coarse grain region adjacent to the fusion line.....	18
Figure 7. Macrograph of experimental weld showing areas (white rectangular boxes) used for characterization of as deposited and reheated WM microstructures and HAZ regions (yellow rectangular boxes). The vertical and horizontal dashed lines indicate the relative positions for the through-thickness and cross-weld microhardness surveys.	19
Figure 8. Macrographs showing hardness indent pattern used for (a) single torch and (b) staggered weld with root, hot and fill pass F1 completed.....	20
Figure 9. Optical micrographs of X100 pipe steel BM near the mid-wall for LPA orientation. (a, b) overall structure, (c, d) mainly bainite, and (e, f) higher proportions of martensite.	21
Figure 10. Through-thickness microhardness traverses for X100 pipe.	22
Figure 11. Optical micrograph showing hardness indents in mainly baintic (286 VHN _{100g}) and predominantly martensitic (369 VHN _{100g}) regions.	22
Figure 12. Representative macrograph of single torch X100 rolled pipe weld 807F.....	23
Figure 13. Representative macrograph of dual torch X100 rolled pipe weld 883D.....	24
Figure 14. WM microstructures of the cap pass in single torch weld 807J.....	25
Figure 15. WM microstructures in underlying fill passes of single torch weld 807J.....	26
Figure 16. WM microstructures of the split cap passes for dual torch weld 883D.....	27
Figure 17: WM microstructure of dual torch pass D4 and the underlying pass D3.	28
Figure 18. HAZ microstructures of the single torch weld 807-J.	29
Figure 19. HAZ microstructures of the single torch weld 807-J.	30
Figure 20. HAZ microstructures of the single torch weld 807-J.	31
Figure 21. HAZ microstructures formed in the dual torch weld 883-D.	32
Figure 22. Microhardness maps for selected single torch pipe welds. Scale units = VHN ₃₀₀	33

Figure 23. Microhardness maps for selected dual torch pipe welds. Scale units = VHN ₃₀₀	34
Figure 24. Cross-weld microhardness traverses for single torch pipe weld, 807-J.	35
Figure 25. Cross-weld microhardness traverses for dual torch pipe weld, 883-D.....	35
Figure 26. Through-thickness microhardness traverses for single torch pipe weld, 807-J.....	36
Figure 27. Through-thickness microhardness traverses for single torch pipe weld, 883-D.	36
Figure 28. Comparison of through-thickness WMC microhardness traverses.	37
Figure 29. Comparison of through-thickness HAZ microhardness traverses.....	37
Figure 30. Macrographs showing (a-f) staggered fill and cap passes in single torch X100 rolled weld, 883J and (g, h) microhardness mapping indent patterns. Pipe wall thickness = 19 mm. ..	38
Figure 31. Detail of staggered fill passes of single torch X100 rolled weld, 883J. Pipe wall thickness = 19 mm	39
Figure 32. Microhardness maps of staggered fill passes (a) F1, (b) F3, (c) F5, and (d) completed weld with cap pass for single torch X100 rolled weld 883J.	40
Figure 33. Macrographs showing (a-f) staggered fill and cap passes in dual torch X100 rolled weld, 883I and (g, h) microhardness mapping indent patterns. Pipe wall thickness = 19 mm....	41
Figure 34. Detail of staggered fill passes in dual torch X100 rolled weld, 883I. Pipe wall thickness = 19 mm	42
Figure 35. Microhardness maps of staggered fill passes (a) D1, (b) D2, (c) D3, (d) D4, and (e) completed weld with cap passes for dual torch X100 rolled weld 883I.	43
Figure 36. Micrographs of as deposited weld metal regions in experimental plate weld NiMo80.	44
Figure 37. Micrographs of reheated WM in experimental plate weld NiMo80.	45
Figure 38. Microhardness results for plate weld NiMo80.	46
Figure 39. Optical micrographs of GHAZ region adjacent to 1.5 kJ/mm deep-fill pass weld in X100-5 steel pipe.	47
Figure 40. Optical micrographs of GHAZ regions adjacent to 0.5 kJ/mm fill passes in X100-5 steel pipe.	48

List of Tables

Table 1. Summary of tests reported	13
Table 2. Chemical composition of X100 pipe and welds	14

1 Introduction

This report provides details of the characterization of experimental girth welds produced for a major consolidated program of research with two primary areas of focus related to the welding of high strength steel pipelines. The first aims to update weld design, testing, and assessment procedures [1]. The second aims to optimize welding solutions for joining high strength steel X100 (Grade 690) pipe by examining the welding process and material variables that lead to variation in weld properties [2]. Characterizing and understanding the microstructures that develop in these high strength steel welds is a key element in the overall investigation to reduce variation in weld properties through better control of the welding process.

It is well known that the microstructures developed in the WM and HAZ regions of high strength pipeline girth welds are dependant on the respective compositions (WM and pipe steel) and the thermal cycle imposed as a result of the specific welding process/procedure that is employed. The factors that influence the weld thermal cycle, and in particular, the cooling time $\Delta t_{800-500}$ (or cooling rate) through the transformation range are critical to understanding microstructure evolution. For welding procedures the major parameters (amperage, voltage, and travel speed) are usually represented by the heat input or more recently by monitoring true energy. Preheat/interpass temperatures and pipe wall thickness also influence the weld thermal cycle and are considered essential welding variables. Understanding the factors that control WM and HAZ microstructures is essential to developing welding procedures that will increase confidence in meeting the stringent mechanical property requirements for strain-based designed pipelines. Requirements for achieving overmatching strength of the WM relative to the parent pipe, while limiting softening in the HAZ are needed to avoid strain localization in a girth weldment. This challenge is even greater with the use of high-productivity advanced pulsed gas metal arc welding (GMAW-P) processes, where multiple-wire process variants still need to be evaluated for their applicability to welding higher strength steel pipe. In response, this program of research emphasizes improved welding procedures and process options in order to meet demanding WM and HAZ mechanical property targets. Many of the details are beyond the scope of this report and may be found in some conference papers [3, 4, 5, 6] and related final reports [7, 8, 9, 10, 11, 12] prepared for other tasks within the consolidated program.

2 Objective

The work reported herein provides an evaluation of the microstructure and hardness of WM and HAZ regions formed in experimental X100 (Grade 690) girth welds and plate welds fabricated under a variety of welding conditions, including single and dual torch variants of GMAW-P. It was intended to establish

- Baseline documentation for microstructures formed with a single pipe composition and a single weld composition, and
- Trends associated with differences in welding practice.

3 Experimental Procedures

Optical microscopy, hardness surveys and detailed microhardness mapping were used to characterize the high strength steel pipe, WM and HAZ regions of experimental rolled and plate welds. Three series of experiments were conducted.

- A total of nine single and dual torch rolled welds were made in 914 mm diameter (36 in. nominal pipe size) by 19.1 mm wall thickness (0.750 in.) X100 (Grade 690) pipe. These baseline welds include six single torch welds identified as 807F through 807K and three dual torch welds identified as 883D, 883E and 883F. Detailed microstructural characterization is reported herein for one single torch weld (807F) and one dual torch weld (883D).
- Two specially designed staggered single and dual torch rolled welds (883I and 883J) were made following the same welding procedures as the nine baseline rolled welds.
- A series of five plate welds were produced for WM thermal simulation experiments. Only the weld produced with the same electrode wire as for the rolled pipe welds is included in this report.

Post weld testing included metallographic examination for microstructure assessment, hardness traverses, and microhardness mapping. The welds and the tests conducted are summarized in Table 1.

3.1 Materials

The same X100 pipe steel and welding consumables were used for all of the welds reported herein and are the same as used for the Round 1 and Round 2 welds discussed in a companion final report [7]. A C-Mn-Si-Ni-Mo-Ti wire electrode in 1.0 mm diameter of ER620S-G (ER90S-G) classification was used for all hot, fill and cap passes. Root passes in the pipe welds were made with a C-Mn ER480S-G (ER70S-G) electrode wire. The pipe was provided by TransCanada Pipelines Ltd. and the welding consumables were provided by CRC Evans.

For pipe welds, samples were taken from three different clock positions, 12:00, 3:00 and 6:00. The samples were surface ground. Pipe and WM were analyzed for all the relevant elements using an OBLF OSG 750 Optical Emission Spectroscope. Chemical analysis was performed on ~20 mm thick transverse macro-sections from each weld. Analysis for C and S was done using LECO CS-600. N and O (WM only) was determined using TC-436 DR analysis. The chemical compositions were used to calculate the carbon equivalents and estimate transformation start temperatures [13].

3.2 Baseline Single and Dual Torch Rolled Pipe Welds

A series of baseline welds was produced that were well controlled and highly monitored, while maintaining essential features of mechanized mainline welding for large diameter pipe. The details of fabrication, welding and weld monitoring are included in reference [7]. Two series of experimental baseline welds, consisting of six single torch and three dual torch rolled (1G) welds, were made under contract at CRC Evans. These welds were fabricated in 1G position by rolling the pipe, Figure 1. This approach minimizes variation in the welding parameters with respect to the clock position and ensures maximum consistency of the deposited WM around the circumference of the pipe. For all pipe welds, a standard fixed-position (5G) root pass procedure was used. Pipe welds were produced in this manner using both single torch and dual torch variants of GMAW-P. Figures 2 and 3 show the joint geometry, pass sequences and representative macrographs for these welds. The single torch welds were completed with the hot pass followed by five fill passes and a cap pass using pulsed-gas metal arc welding (GMAW-P). In the case of the dual torch welds, the hot pass was followed by two dual torch runs (denoted D1- D2 and D3-D4 in Figure 2 (b)), a fifth single torch fill pass (F5) and two final split cap passes also employing GMAW-P. A minimum preheat temperature of 100°C and maximum interpass temperature of 125°C were closely monitored and maintained throughout welding. The welding

parameters were monitored through the welding system as well as by an external data acquisition system. The weld thermal cycles were also acquired using a large number of thermocouples, both in-situ (predrilled to target the HAZ close to the fusion line) and plunged into the weld pool of selected fill passes.

3.3 Staggered Single and Dual Torch Rolled Pipe Welds

The work on full pipe welds was supplemented by a series of staggered-bead pipe welds. The staggered-bead pipe welds provided a systematic assessment of microstructure development with the deposition of successive weld beads. The same procedure as described above was used. However, in this case, each individual fill and cap pass was stopped short of completing the full pipe circumference at predetermined clock positions. This left some length of each weld pass (300 to 400 mm) as-deposited (AD) without refinement by subsequent weld passes. This approach of staggering the weld pass sequence allowed for post-test analysis of each pass in both as-welded and reheated conditions. Figure 4 shows examples of the partially filled staggered welds that were prepared for analysis including detailed microhardness mapping.

3.4 Single Torch Plate Weld

The work on full pipe welds was supplemented also by a series of flat plate welds using the pipe steel remaining from the rolled welds. The primary purpose of these welds was to create AD WM for Gleeble®¹ test specimens to be used in the WM physical simulation studies. It was determined during the initial evaluation of these welds that they provided an excellent opportunity to assess both WM and HAZ microstructure and hardness for two distinctly different welding procedures in the same pipe material. Consequently, the plate weld representing the C-Mn-Si-Ni-Cr-Mo-Ti ER62S-G (ER90S-G) wire electrode used in the rolled pipe welds was also used here to bring additional insight to the microstructure evaluation. Pipe was cut and flattened. Weld test assemblies were prepared with the same joint geometry used for the pipe welds as shown in Figure 2. The weld was produced using a pass sequence that consisted of a hot pass at a heat input of 0.2 kJ/mm, followed by three standard fill passes at a heat input of 0.5 kJ/mm to fill about 50% of the joint. Up to this point, the welding procedures were the same as for the pipe welds. The final deep-fill pass was deposited at a heat input of 1.5 kJ/mm to complete the experimental plate weld (Figure 5). The plate weld assembly was intentionally allowed to cool to ambient temperature prior to deposition of the final deep-fill pass to ensure the fastest cooling possible for the heat energy input used. Further details are provided in another final report [8].

3.5 Metallography and Microhardness Traverses

All metallographic specimens were prepared using standard semi-automatic metallographic techniques. For the X100 pipe steel base metal, full thickness sections were cut longitudinal to the pipe axis (LPA) and transverse to the pipe axis (TPA) to provide an assessment of the microstructure for the full wall thickness of the pipe. For the welds, the full cross-sections were cut from the experimental welds and surface ground. The specimens were mounted in epoxy resin and further ground and subsequently polished using a series of diamond suspensions and a final polish with a 0.05 µm colloidal silica suspension. All specimens were etched in 3% Nital solution to reveal the microstructure of the WM and HAZ. Representative macrographs and several micrographs were taken at a range of magnifications to

¹ Gleeble® is a registered trademark of Dynamic Systems Inc. Corporation New York P.O. Box 123, Route 355 Poestenkill New York 12140

assess different through-thickness positions in the WM and HAZ regions of the single and dual torch X100 rolled welds.

A representative macrograph with the locations (white and yellow rectangular boxes) selected for examination of WM and HAZ regions in the 1.5 kJ/mm deep-fill and underlying 0.5 kJ/mm fill passes is shown in Figure 7. Both AD and reheated regions were characterized and several images were recorded at a range of magnifications to help quantify the constituent phases formed within the respective regions. In selected cases, further details of the fine-scale microstructures were revealed using scanning electron microscopy. The International Institute of Welding (IIW) classification scheme [14] is used in conjunction with modification proposed by Thewlis [15]. The valuable review on classification and quantification of microstructures in steels greatly aids evaluation of complex WM and HAZ structures.

Microhardness traverses (dotted white lines) were carried out using a diamond pyramid indenter with a 300g force and spacing between indents of ~0.5 mm. Through-thickness and cross-weld hardness surveys were made in the positions shown in Figure 6.

In the process of conducting microstructure evaluations, supplementary microhardness measurements of specific phases were conducted using a diamond pyramid indenter with a 100g force.

3.6 Microhardness Measurement and Mapping

Microhardness measurements were conducted for purposes of producing a hardness plot. These plots provide a visual image of the hardness distribution in each sample. Samples were removed from the welds in the same manner as for metallography and hardness traverses. Sample preparation was conducted in a manner to minimize the potential influence of grinding, polishing and etching on the measurements.

3.6.1 Sample Preparation

The microhardness samples were mounted in a phenolic hot mount resin and ground flat utilizing an 80 grit resin bonded diamond disk. After grinding, a series of progressively finer diamond grits were utilized to remove the effects of the mechanical grinding. The last step with 1200 grit, prepared the sample for diamond polishing. All of the grinding steps used water lubrication. The samples then were polished using 6 μm followed by 3 μm diamond on Struers MD-Plus. The final polish was a 1 μm diamond on Struers MD Nap. All of the diamond polishing was done with a water-based lubrication medium containing anti-corrosion additives. This was followed by hot air drying and storage in a controlled-humidity desiccator until ready to proceed with hardness measurements. All samples were cleaned with soapy water, rinsed in tap water and re-rinsed with denatured methanol after each diamond size.

Just prior to indenting, each sample was removed from the desiccator, etched with 10% Nital and then digitally photographed on a copy stand. To improve hardness measurement accuracy, the sample then was re-polished to remove the etching immediately prior to measurement.

3.6.2 Measurement and Mapping

Each prepared sample was mounted in a self-levelling holder for hardness measurements utilizing a Matsuzawa Digital Vickers Hardness Tester (model VMT-72) operated by Clemex software. The

standard diamond pyramid indenter was loaded with a preselected force of 300 g. To prevent faulty measurements caused by induced work hardening from previous indents, a spacing of 300 μm between indents and edges was selected. This exceeds the recommended 3x diagonal spacing between indent centers and the 2.5x diagonal spacing recommended for eliminating edge effects. The indenter dwell time was set at 11.5 s.

For each fully welded pipe sample, this procedure resulted in a base grid pattern of 60 x 50 on a fully welded specimen. The depth of the grid was modified for each sample to include the entire weld cap pass and root pass. Similarly for each staggered pipe weld, the base grid was adjusted to suit the reduced weld thickness and then supplemented to include the HAZ above the last weld pass in each macro-section. Thus, varying grid sizes and the number of indents was altered to accommodate each weld. Representative grid patterns are illustrated in Figure 8.

The starting measurement position on each sample was chosen by examining the HAZ visible in the macrograph relative to the weld cap or last pass deposited. For fully welded joints, the starting point was 10 mm away from the intersection of the weld cap edge with base pipe surface. A similar point was selected on the other side of the weld to define the length of the grid. For staggered weld sections, the starting point was selected in similar manner, but using the fusion boundary at the top of the last weld pass deposited in lieu of the cap pass. This procedure was sufficient to ensure representative sampling of base metal, HAZ, fusion zone and WM on both sides of the weld centerline.

After the data was checked and processed, the sample was re-etched with 10% Nital and a second macrograph was taken to ensure all of the critical features were properly sampled. If necessary, the data was discarded and the sample was prepared again by grinding the indents out, re-polishing and rerunning with a larger grid. At the conclusion of each experiment, the data was reviewed for mis-readings, unequal diagonals or abnormal readings. Each suspect reading was manually re-measured. The data was collected as an Excel file containing sample identity, position, measured Vickers hardness and both diagonals. Post-test data processing in Excel was used to create individual color maps with a hardness interval fixed to ten points per colour code.

4 Results and Discussion

4.1 X100 Pipe Steel

The development and evolution of high strength pipe steels has been greatly enhanced by application of advanced thermo-mechanical controlled processing (TMCP) in conjunction accelerated cooling to obtain desired microstructures [16, 17, 18, 19]. The pipe used for this investigation is representative of the more recent evolutions in pipe steel development.

Table 2 lists the chemical composition of pipe and pipe welds evaluated in this investigation. For the X100 pipe steel BM, full thickness sections were cut longitudinal (parallel) and transverse to the pipe axis (LPA and TPA orientations) to provide an assessment of the microstructure for the full wall thickness of the pipe. There is variation in microstructure observed from the outer and inner diameter (OD and ID) surfaces towards the central mid-wall region where a more banded structure exists. Some examples of the range of microstructures observed in the mid-wall position are shown in Figure 9.

It can be seen that through-thickness microstructural variation exists where there are areas of predominantly bainite towards the OD and ID and increased proportions of martensite near the mid-wall

region. The variation in microstructure correlates reasonably well with the through-thickness microhardness measurements that were made on both LPA and TPA specimens, as illustrated in Figure 10. As seen there is higher microhardness toward the OD and ID surfaces and occasional high hardness at the pipe mid-wall region where the banded microstructure was observed. The marked differences in microhardness between the mainly bainitic (286 VHN_{100g}) and martensitic (369 VHN_{100g}) regions is illustrated in Figure 11, where the indents were accurately placed in the respective phases.

4.2 Single And Dual Torch Rolled X100 Welds

Figures 12 and 13 show representative macrographs of the single and dual torch rolled X100 welds. From these figures several important features are revealed, including aspects related to the macrostructure, the relative distribution of AD and reheated regions, the profile of the fusion line and the width of the HAZ regions within the pipe steel material. In the single torch weld the overall columnar structure is seen to extend from the fusion line towards the weld centerline in the majority of fill passes and ends up being essentially vertical in the cap pass (Figure 12). Reheated regions appear as slightly darker bands which are evident between the passes including beneath the cap pass. At this magnification the columnar structure appears to extend unaltered through the reheated bands. This observation is important since distinguishing between the AD and reheated regions becomes very difficult for high strength WM. Since the weld torch is oscillated during welding to improve fusion with the side wall, the fusion line tends to have a wavy profile as does the visible HAZ. Notice the light-etching relatively narrow grain coarsened HAZ regions immediately adjacent to the fusion line. The most obvious differences seen for the dual torch weld (Figure 13) relate to the bead shape and fusion line profile as well as the relative distribution of AD and reheated regions. Also important is the marginally wider coarse region next to the fusion line and overall extent of the visible HAZ. Again a WM columnar structure dominates and there is only a faint demarcation between the lead and trail beads of a given dual torch run. Generally wider reheated bands are observed especially beneath the cap pass where a significant amount of reheated WM was found.

Detailed characterization of the microstructural features of single and dual torch rolled X100 welds was carried out at CANMET to provide information on the consistency of the welding procedures and to identify the major variations in microstructure and microhardness among the welds. The complex relatively fine microstructures formed in high strength weld metals makes precise classification more difficult. In addition, the WM and HAZ regions contain areas that have experienced single or multiple thermal cycles as a result of the multipass welding techniques employed. This can produce subtle to marked differences in the morphology of transformed microstructures as a result of small changes in the thermal cycle experienced in a given location. Additional work by Fairchild et al. [20] further illustrates the complexities and range of phases and detailed constituents formed in high strength weld metals by employing not only optical microscopy but also advanced characterization techniques. Further dilatometric and microstructural data to study the transformation behaviour of selected high strength weld metals using thermal simulation techniques is reported by Gianetto et al [8].

For example, obvious microstructural differences between the cap pass and underlying passes are often observed, as evidence in Figures 14 and 15 for the single torch weld. The as deposited WM region of the cap pass has a columnar structure with prior austenite grains delineated by continuous or discontinuous grain boundary ferrite (GF) and/or occasional aligned ferrite-with second phase (upper bainite) (FS(A)). A comparatively fine martensite/bainite/acicular ferrite mixed microstructure formed within the grain interiors. In some areas, intercritical reheating occurred (Figure 14(b)) where prior austenite grain boundaries are delineated by second phase resulting from the partial re-austenitization

and subsequent cooling. In this case the grain interiors exhibit slightly coarser bainite/acicular ferrite lath-like structure with martensite also present. Other underlying fill passes (F4, F3, and F2) shown in the micrographs in Figure 15 have fine lath structures that are not as well defined compared to the cap pass microstructure. Very little grain boundary phases exist and distinguishing between AD and reheated regions becomes very difficult with only subtle changes being observed.

The dual torch weld procedure had a relatively large torch separation (distance between the lead and trail wires of 121 mm (4.75 in.)), and used two dual torch runs with a single torch F5 (Figure 2) that was followed by offset dual torch cap passes to complete the weld. An important observation is the marginally coarser microstructure observed for the trail pass compare to the lead pass, as evident in Figures 16 and 17. The lead cap pass microstructure is similar to single torch weld in terms of observed phases with relatively narrow columnar grains delineated by continuous and discontinuous GF as well as FS (A) (Figure 14(a) compared to Figure 16(b)). The grain interiors have a fine lath structure with occasional polygonal ferrite. Figure 17 shows the underlying WM structures of the second dual torch run; weld passes D3 and D4 where it is clear that the trail bead (D4) exhibits a coarser overall microstructure relative to the lead pass (D3). This is consistent with the higher effective local preheat temperature that exists because of the short time between the deposition of the lead wire and the trail wire. This produces slower cooling conditions (increased cooling time) for the trail bead. Further observations of the differences and similarities between the single and dual torch WM are provided in sections dealing with the staggered welds where hardness data also supports these observations.

The variation in microstructures formed in the HAZ regions of the single torch pipe weld is seen in the micrographs in Figures 18 to 20. Again, differences relate to the complex thermal cycles that occur in the HAZ region adjacent to the fusion line [9, 16, 17]. The three regions near the fusion line that were identified and examined include the grain coarsened (GC) HAZ, supercritically-reheated GCHAZ and intercritically-reheated (ICR)-GCHAZ regions. The GCHAZ region microstructure varied from positions beneath the cap pass and underlying fill passes although there was obvious ICR-GCHAZ regions observed, as shown in Figure 18. Beneath the cap pass a mixed microstructure was observed with the equiaxed prior austenite grains sometimes delineated by GF or FS (A), while the grain interiors consisted of fine bainite and lath martensite. In contrast, a relatively coarser, predominantly bainitic structure was formed in the delineated ICR-GCHAZ grains in Figure 18(b). In Figure 19, a supercritically reheated GCHAZ region with partial grain refinement was found near fill pass F4. There was a large variation in the size and shape of re-transformed grains that exhibited a mainly bainitic structure with occasional polygonal ferrite. In other areas, inter-critical reheating was frequently observed that, depending on the peak temperature reached caused varying degrees of delineation of prior austenite grain boundaries (Figure 19(b)). In the HAZ near F2 the microstructure was quite variable in terms of overall grain structures with fine regions and mixed coarser bainitic packets evident (Figure 20). The major differences observed for the dual torch weld are evident in the micrographs, shown in Figures 21. The ICR-GCHAZ and GCHAZ regions with relatively coarse grains contained comparatively coarse bainitic-ferrite laths formed in packets within the prior austenite grains. Adjacent to both the cap and root passes the ICR-GCHAZ had dark second phase present at the grain boundaries. More detailed characterization of GCHAZ microstructure and properties in three X100 pipe steels is presented in a companion report [9].

To further characterize the degree of microstructural variation in the experimental welds complete microhardness maps were created for both series of rolled pipe welds. For the single torch pipe welds there was a relatively consistent pattern of hardness that corresponds well with the distribution of AD and reheated regions within the welds (Figures 22 and 23). The alternating pattern of high hardness AD

regions and softer reheated regions is clearly evident. There is a tendency for more slivers of AD to be retained in the hot and first few fill passes compared to the last fill passes beneath the high-hardness cap pass. It is also clear that the HAZ region is considerably softer than the WM. In the dual torch welds there was some inconsistency with respect to the microhardness maps. In some instances, they were very similar to the single torch, while in other cases more uniform hardness was observed along with a wider HAZ region.

The supplementary microhardness testing completed at CANMET revealed some interesting trends as seen in the cross-weld and through-thickness traverses in Figures 24 to 27. For both the single and dual torch welds, cyclic saw-tooth-type hardness profiles were observed. In the cross-weld traverses there was little difference in the level of hardness between the sub-cap and mid-wall locations although in the latter case the profile was narrower. The marked decrease in hardness between the WM and softened HAZ is clearly revealed. The profiles were not always symmetrical in terms of HAZ and pipe base metal profiles as evident in Figures 24 and 25. In the case of the single torch pipe weld (Figure 24) the right side of the profile had very high hardness that is consistent with the results presented for the pipe steel in Figure 10, where it was clearly shown that high hardness values were related to martensitic regions near the pipe mid-wall location. For the dual torch, the profiles are much more cyclic within the WM regions and there is slightly lower overall hardness ($<240 \text{ VHN}_{300g}$) in the softened HAZ. For the sub-cap profile the high hardness on the left side occurred because the cap pass extended much further over the pipe base metal on the outside surface and a GHAZ region was formed that was essentially parallel to the OD surface.

The through-thickness WM and HAZ hardness profiles in Figures 26 and 27 shows the cyclic or oscillating nature of the hardness profiles, which correspond with the variation in thermal cycle that occurs throughout the entire weld. In both cases (single and dual torch) relatively high hardness exists in the vicinity of the cap passes. Reheating of the underlying material produces significant softening that is more pronounced in the HAZ regions. The cyclic or saw-tooth profiles are observed throughout the pipe wall thickness. Profiles for the dual torch welds tend to have wider peaks and valleys. Superimposing the through-thickness WM and HAZ hardness profiles (Figures 28 and 29) for each process variant illustrates the differences and similarities between the pipe welds.

4.3 Staggered Single and Dual Torch Rolled X100 Welds

The staggered welds were used to determine the relative pass thickness and to qualitatively determine the ratio of AD and reheated that exist in single and dual torch welds. In the macrographs presented in Figures 30 and 31 for a single torch weld the light bands represent the extent of each weld bead including the visible reheated zone in the underlying pass. They tend to be farther apart toward the hot and initial fill passes and end up being closer together towards the top where the fifth fill pass is largely reheated by the cap pass (Figures 30(e) and (f)). As a result, the single torch weld exhibits an alternating pattern of AD and reheated WM toward the root which is illustrated in the series of microhardness maps in Figure 32. Two important observations are apparent from these images. First, the AD WM exhibits relatively high hardness and deposition of successive beads reheats a small portion of the underlying pass. The influence of reheating is more pronounced for the third fill pass and above. This helps to explain why higher strength has been measured for tensile specimens biased towards the mid-wall/hot pass of mechanized single torch girth welds [21, 22, 23, 24, 25].

In the case of the dual torch weld, the interaction of the two wires (weld pools) is dependent on the spacing between the electrode wires and the travel speed and this greatly affects the resultant WM and

HAZ regions. With one dual torch run, two passes are deposited together and effectively appear to be one pass that is slightly thinner than two single torch weld passes. The pass sequence and weld deposition are shown in Figures 33 and 34. On a macro-scale there is very little evidence of the lead wire pass since the trail wire is effectively melting and reheating the underlying pass as illustrated in the sections for D2 and D4. A fifth fill pass was deposited with a single torch and it can be seen that this also reheated a great deal of the underlying D4 pass. Application of a split offset cap essentially reheats the entire fifth fill pass. It is worth noting that the second cap pass produces a much larger WM reheated zone than the HAZ in the adjacent pipe material (see Figure 33(f)). This illustrates that a much higher effective local interpass temperature exists from deposition of the weld pass via the lead wire. In the expanded macrographs in Figure 34, the development of the dual torch weld becomes more evident by comparing the sections from D1 through D4. The extent of reheating is evident in both the WM and adjacent HAZ, where it is clear that the trailing wire significantly melts into the underlying pass effectively leaving what appears to be a single weld bead. A small line may be seen between the beads but in most cases it looks like the deposit is made up of one pass (bead). The hardness maps in Figure 35 also illustrate the evolution of the dual torch weld. Similar to the single torch, the lead wire pass initially exhibits high hardness that is in many cases completely reheated or softened by the deposition of the second pass of the trailing wire. In the completed dual torch weld a much more uniform through-thickness hardness distribution is observed than in the single torch case.

4.4 Single Torch X100 Plate Welds

For the experimental plate weld, a comparison between the microstructure and microhardness of the 1.5 kJ/mm deep-fill pass and underlying 0.5 kJ/mm fill passes was carried out to provide a better understanding of their respective transformation behaviours for two different thermal cycles. This also may offer insight into the potential influence of single pass versus multipass welding. Results are summarized to show specific trends observed for the WM and provide an assessment of the HAZ generated in the pipe steel as a function of heat input. The complete set of data is presented in a consecutive final report [8]. Representative micrographs of the as deposited (AD) and reheated regions of the 1.5 kJ/mm deep-fill pass are compared to the corresponding regions of the underlying 0.5 kJ/mm fill passes in Figures 36 and 37. The 1.5 kJ/mm deep-fill pass exhibited a mainly AF structure with some discontinuous GBF or FS (A) or FS (N) (upper bainite). In contrast, the very narrow prior austenite grains within the lower-energy-input weld transformed to a much finer high hardness (average; 332 to 342 VHN_{300g}) martensitic/ bainitic microstructure. Again there was a wider range of hardness and correspondingly higher variation for the low-heat-input multipass weld region. As indicated above, the influence of reheating in the low-energy-input weld is reflected in the alternating pattern of higher and lower hardness values, as shown in Figure 38. It is also important to notice that reheated WM generated by deposition of the 1.5 kJ/mm deep-fill pass resembles the AD microstructure formed within it (compare Figures 36(b) and 37(b)).

Representative micrographs of the HAZ regions adjacent to the fusion line for both the 1.5 kJ/mm and underlying multipass 0.5 kJ/mm weld passes, are shown in Figures 39 and 40. The GCHAZ region adjacent to the 1.5 kJ/mm weld pass transformed to a range of structures, including upper bainite, along with smaller packets of finer bainite and some occasional intragranular bainitic regions. Referring back to the hardness traverse data in Figure 38, it can be seen that the HAZ of the 1.5 kJ/mm weld is wider and has hardness values close to those of the WM (between 260 and 280 VHN_{300g}). In the multipass lower heat input (0.5 kJ/mm) region the extent of the entire HAZ can be seen in Figure 40(a) and the very narrow region adjacent to the fusion line is not as coarse as for the 1.5 kJ/mm case. Three regions near the fusion line were observed, including GCHAZ (Figure 40(b)), supercritically-reheated GCHAZ

(Figure 40(c) and (d)) and intercritically-reheated GCHAZ regions (Figure 40(e) and (f)). In the GCHAZ region, an overall finer structure exists within the equiaxed prior austenite grains. The mixed structure contains both martensite and bainite. Varying amounts of refinement occurred in the supercritically reheated region that are dependent on the peak temperature reached and the time at this temperature [16, 17]. Exposing GCHAZ grains to temperatures within the intercritical range produced varying degree of delineation of prior austenite grain boundaries with second phase constituents, which results from partial re-austenitization and subsequent cooling.

5 Summary and Conclusions

In this study, the WM microstructures formed in single and dual torch GMAW-P X100 pipe welds were characterized using conventional metallographic methods and mapping of microhardness across the entire weld region. Significant variation in the microstructural constituents was observed in both the WM and the HAZ, particularly at the faster cooling rates typical of narrow gap GMAW-P pipeline girth welds. The microstructural changes occurred over very short distances making any assessment of potential influence on overall weld performance more difficult. Some of the observations and conclusions that can be drawn from this evaluation include:

1. There is considerable local variation in microstructure for the relatively fast cooling conditions that exist in the narrow gap pipe welds produced with single and dual torch process variants.
2. The complex WM microstructures formed in the single torch pipe welds consisted of mixed bainite/martensite with higher hardness in AD compared to reheated regions. Cyclic hardness profiles result from reheating and tempering of the underlying WM. In the dual torch pipe welds, higher hardness of the lead wire deposit is significantly altered by deposition of the trail wire.
3. Three HAZ structures/regions formed in the multipass pipe welds include the GCHAZ, supercritically reheated GCHAZ and ICR-GCHAZ. The microstructures formed within these regions are consistent with the cyclic variation in through-thickness hardness and resultant constituent phases formed within the respective regions.
4. Staggered welds proved useful for developing a better understanding of the evolution of microstructure with successive weld passes. They clearly show the range of weld bead thicknesses, the relative distributions of AD and reheated WM the changes in WM and HAZ microhardness that occur with deposition of successive weld passes (influence of reheating and tempering).
5. Microhardness maps give a good visual indication of the hardness distribution, especially in the WM region where reheated zones are difficult to distinguish by conventional metallographic examination.
6. Cross-weld and through-thickness microhardness traverses illustrate the relative changes in hardness as a function of local thermal cycle and allow specific regions such as the GCHAZ to be better quantified. For example, the lower through-thickness HAZ hardness compared to the WM provides a good indication of the specific regions relative tensile properties.
7. Detailed evaluation of high strength pipe and various welds in this investigation has illustrated some of the limitations of conventional metallographic examination for characterizing the very fine WM and HAZ microstructures formed in advanced pipeline girth welds.

6 Acknowledgments

This research was funded, in part, by CANMET-MTL and the Federal Program for Energy Research and Development. The authors would like to thank CANMET-MTL staff, including Mr. M. Kerry for his machining expertise, Mr. R. Eagleson for performing mechanical testing, and Ms. P. Liu and Ms. R. Zavadil for expert metallographic analysis and microhardness testing. The technical expertise of Mr. M. Carroscia and Mr. Frank Karl, Lincoln Electric, is also appreciated. This research is part of a consolidated program jointly funded by the Pipeline and Hazardous Materials Safety Administration of the U.S. Department of Transportation (DOT), and the Pipeline Research Council International, Inc. (PRCI).

7 References

1. DOT-PRCI, 2007-2011 “Update of Weld Design, Testing, and Assessment Procedures for High Strength Pipelines,” <http://primis.phmsa.dot.gov/matrix/PrjHome.rdm?prj=225>.
2. DOT-PRCI, 2007-2011 “Development of Optimized Welding Solutions for X100 Linepipe Steel,” <http://primis.phmsa.dot.gov/matrix/PrjHome.rdm?prj=226>.
3. Chen, Y., Wang, Y., Gianetto, J., Rajan, V., Quintana, M., “Simulation of Microstructure Evolution and its Experimental Verifications for Girth Welds in High-Strength Pipelines,” International Pipeline Conference, ASME, IPC2010-31374, pp. 1-6, September 27– October 1, 2010.
4. Gianetto, J., Tyson, B., Wang, Y.-Y., Bowker, J., Park, D., and Shen, G., “Properties and Microstructure of Weld Metal and HAZ Regions in X100 Single and Dual Torch Girth Welds,” International Pipeline Conference, ASME, IPC2010-31411, pp. 1-11, September 27– October 1, 2010.
5. Rajan, V., Chen, Y. and Quintana, M., “A New Approach to Essential Welding Variables in Girth Welding of High Strength Pipe Steels,” International Pipeline Conference, ASME, IPC2010-31374, pp. 1-8, Calgary, Alberta, Canada, September 27– October 1, 2010.
6. Wang, Y.-Y., Liu, M., Gianetto, J. and Tyson, B., “Considerations of Line Pipe and Girth Weld Tensile Properties for Strain-Based Design of Pipelines,” International Pipeline Conference, ASME, IPC2010-31376, pp. 1-10, Calgary, Alberta, Canada, September 27– October 1, 2010.
7. Panday, R. and Daniel, J., “Materials Selection, Welding and Weld Monitoring”, Final Report 278-T-02 to PHMSA per Agreement # DTPH56-07-T-000005, September 2011.
8. Gianetto, J.A., Goodall, G.R., Tyson, W.R., Quintana, M.A., Rajan, V.B. and Chen, Y., “Microstructure and Properties of Simulated Weld Metals”, Final Report 278-T-04 to PHMSA per Agreement # DTPH56-07-T-000005, September 2011.
9. Gianetto, J.A., Goodall, G.R., Tyson, W.R., Quintana, M.A., Rajan, V.B. and Chen, Y., “Microstructure and Properties of Simulated Heat Affected Zones”, Final Report 278-T-05 to PHMSA per Agreement # DTPH56-07-T-000005, September 2011.
10. Rajan, V.B., “Essential Welding Variables”, Final Report 278-T-09 to PHMSA per Agreement # DTPH56-07-T-000005, September 2011.
11. Chen, Y., Wang, Y.-Y., Quintana, M.A., Rajan, V.B. and Gianetto, J.A., “Thermal Model for Welding Simulations”, Final Report 278-T-07 to PHMSA per Agreement # DTPH56-07-T-000005, September 2011.
12. Chen, Y., Wang, Y.-Y., Quintana, M.A., Rajan, V.B. and Gianetto, J.A., “Microstructure Model for Welding Simulations”, Final Report 278-T-08 to PHMSA per Agreement # DTPH56-07-T-000005, September 2011.

13. W. Steven and A. G. Haynes, "The Temperature of Formation of Martensite and Bainite in Low-Alloy Steels," *Journal of Iron and Steel Research International*, 1956.
14. 'Compendium of weld metal microstructures and properties'; Abington, Woodhead Publishing, 1985.
15. Thewlis, G., "Materials Perspective – Classification and Quantification of Microstructures in Steels," *Materials Science and Technology*, Vol. 20, pp. 143-160, 2004.
16. Collins, L. E., Godden, M.J. and Boyd. J.D., "Microstructures of Linepipe Steels", *Canadian Metallurgical Quarterly*, Vol. 22, No. 2, pp. 169-179, 1983.
17. Hudson, M.G., "Welding of X100 Linepipe," Ph.D. Thesis, Welding Engineering Research Centre, Cranfield University, 2004.
18. Hillenbrand H-G. and Kalwa C., "Production and service behaviour of high-strength large-diameter pipe", *Proceedings of Pipe Dreamer's Conference, Application and Evaluation of High-Grade Linepipes in Hostile Environments*, Yokohama, Japan, 7-8 November 2002, pp. 203-215, 2003.
19. Hara, T., Terada, Y., Shinohara, Y., Asahi, H., and Doi, N., "Metallurgical Design and Development of High Deformable X100 Line Pipe Steels Suitable for Strain-Based Design," 7th Int. Pipeline Conf., ASME, IPC2008-64234, pp.1-7, 2008.
20. Fairchild, D., Macia, M., Bangaru, N., Koo, J., Ozekcin, A., and Jin, H., "Welding Development for the World's Strongest Pipeline: X120," 7th International Conference on Trends in Welding Research, ASM International, May 16-20, 2005, Pine Mountain, Georgia, USA, pp. 749-754, 2005.
21. Gianetto, J.A., Bowker, J.T., Bouchard, R., Dorling, D.V. and Horsley, D., "Tensile and Toughness Properties of Pipeline Girth Welds," *Welding in the World*, Vol. 51, No. 5/6, pp. 64-75, 2007.
22. Fiore, S. R., Gianetto, J.A., Hudson, M. G., Vase, S., Khurana, S., Bowker, J.T. and Dorling, D.V., "Development of Optimized Weld Metal Chemistries for Pipeline Girth Welding of High Strength Line Pipe," 7th Int. Pipeline Conf., ASME, IPC2008-64593, pp. 1-12, 2008.
23. Gianetto, J.A., Bowker, J.T., Dorling, D.V., Taylor, D., Horsley, D. and Fiore, S.R., "Overview of Tensile and Toughness Testing Protocols for Assessment of X100 Pipeline Girth Welds", 7th Int. Pipeline Conf., ASME, IPC2008-64668, pp. 1-10, 2008.
24. Hamada, M., Shitamoto, H. and Hirata, H., "Tensile Properties and Microstructure of Girth Welds for High Strength Linepipe," *Proc. of 19th Int. Offshore and Polar Eng. Conf., ISOPE*, Osaka, Japan, pp. 50-55, 2009.
25. Gianetto, J.A., Tyson, W.R., Park, D.Y., Shen, G., Lucon, E., Weeks, T.S., Quintana, M.A., Rajan, V.B. and Y.-Y. Wang, "Small Scale Tensile, Charpy V-Notch, and Fracture Toughness Tests", Final Report 277-T-05 to PHMSA per Agreement # DTPH56-07-T-000005, September 2011.

Table 1. Summary of tests reported

Sample ID	Metallography	Microardness	
		Traverse	Detailed Map
SINGLE TORCH ROLLED PIPE WELD			
807F	Macrostructure Microstructure	Through thickness Cross weld	Yes
807K	Microstructure	Through thickness Cross weld	Yes
807J		Through thickness Cross weld	Yes
DUAL TORCH ROLLED PIPE WELD			
883D	Macrostructure Microstructure	Through thickness Cross weld	Yes
883F			Yes
STAGGERED BEAD ROLLED WELDS			
833I - single torch	Macrostructure Microstructure		Yes
883J - dual torch	Macrostructure Microstructure		Yes
SINGLE TORCH PLATE WELD			
X100-03	Microstructure	Through thickness Cross weld	No

Table 2. Chemical composition of X100 pipe and welds

Element	X100 Pipe	Single Torch Pipe Weld	Dual Torch Pipe Weld	X100 Plate Weld
C	0.07	0.114	0.112	0.100
Mn	1.83	1.38	1.48	1.4
Si	0.11	0.54	0.56	0.49
S	0.005	0.012	0.011	0.012
P	0.005	0.013	0.014	0.012
Ni	0.52	0.95	0.99	0.89
Cr	0.03	0.05	0.07	0.05
Mo	0.27	0.35	0.36	0.34
Cu	0.30	0.13	0.14	0.16
Al	0.04	0.006	0.005	0.007
Nb	0.027	0.003	0.006	0.008
Ti	0.009	0.032	0.038	0.029
O	-	0.0230	0.032	0.045
N	0.004	0.0081	0.004	0.0072
CE_{IW}	0.49	0.50	0.52	0.48
P_{CM}	0.21	0.25	0.26	0.23
CEN	0.31	0.39	0.41	0.35
B_s	603	607	595	612
M_s	452	437	433	444

Notes:

$$B = <0.0005$$

$$CE_{IW} = C + Mn/6 + (Cr+Mo+V)/5 + (Ni + Cu)/15$$

$$P_{cm} = C + Si/30 + (Mn+Cu+Cr)/20 + Ni/60 + Mo/15 + V/10 + 5B$$

$$CEN = C + A(C) \times (Si/24 + Mn/6 + Cu/15 + Ni/20 + (Cr+Mo+Nb+V)/5 + 5 \times B)$$

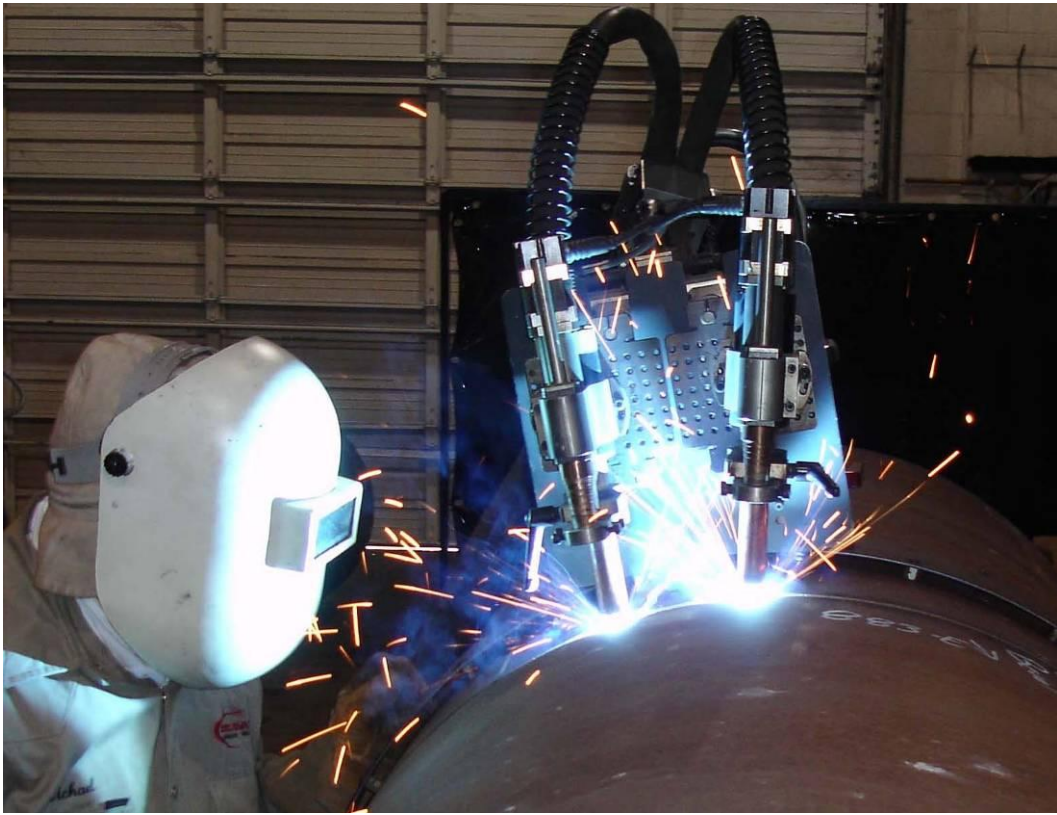
$$\text{where } A(C) = 0.75 + 0.25 \tanh\{20 \times (C - 0.12)\}$$

$$B_s = 830 - 270(C) - 90(Mn) - 37(Ni) - 70(Cr) - 83(Mo)$$

$$M_s = 561 - 474(C) - 33(Mn) - 17(Ni) - 17(Cr) - 21(Mo)$$

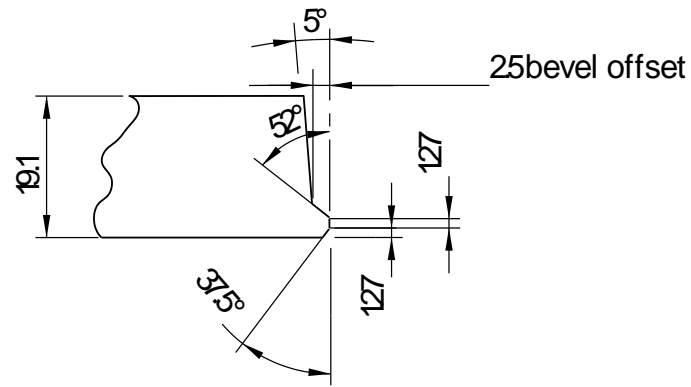


(a)

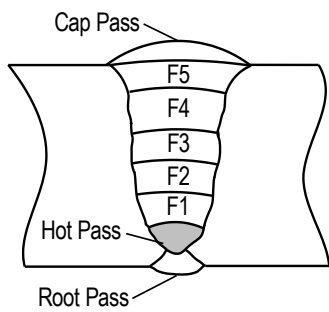


(b)

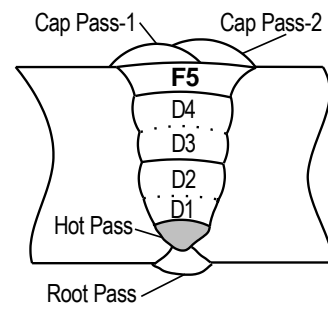
Figure 1. Single and dual torch roll welding.



(a) Schematic of pipe end joint geometry (dimensions in mm).

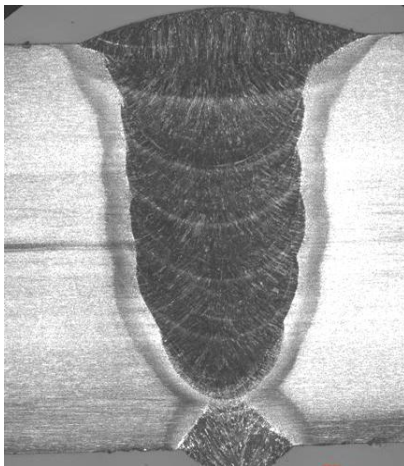


(b) single torch pass sequence

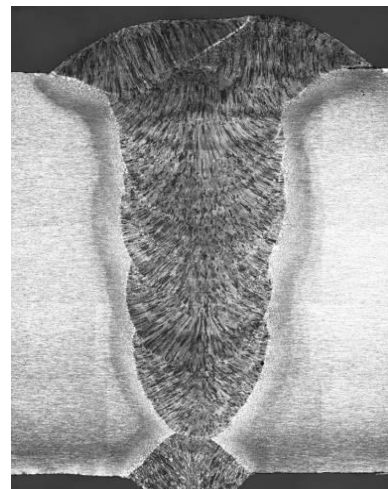


(c) dual torch pass sequence

Figure 2. Schematic diagrams of joint geometry and pass sequences used for pipe welds.



(a) Single torch (807-F), X3.



(a) Dual torch (883-F), X3.

Figure 3. Representative macrographs of single and dual torch pipe welds. (Pipe wall thickness = 19 mm)

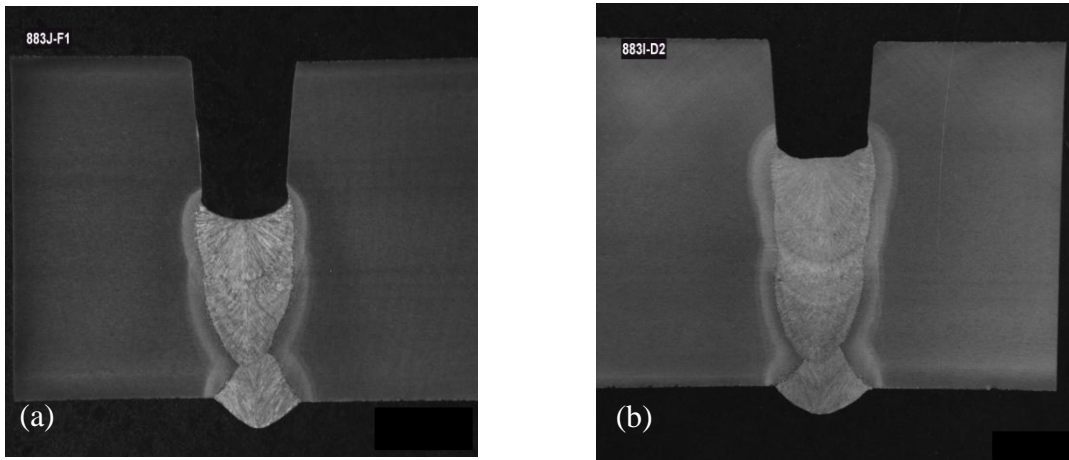
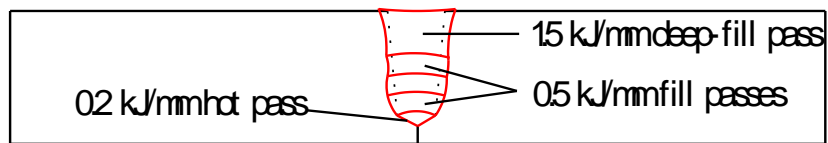
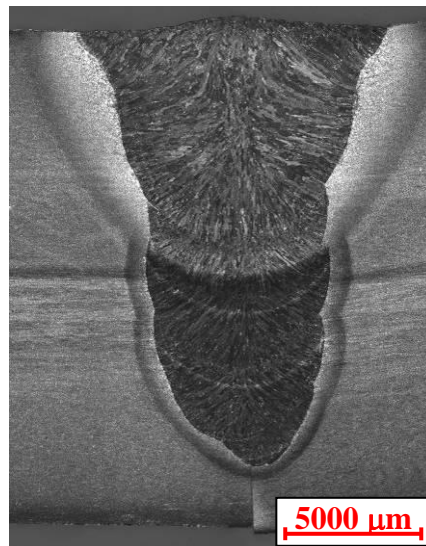


Figure 4. Macrographs of staggered weld passes (a) single torch fill pass (F1) and (b) dual torch fill passes D1 and D2. X~2.5



(a) Weld pass sequence.



(b) Macrograph

Figure 5. Schematic of pass sequence (a) and macrograph of experimental plate weld (b).

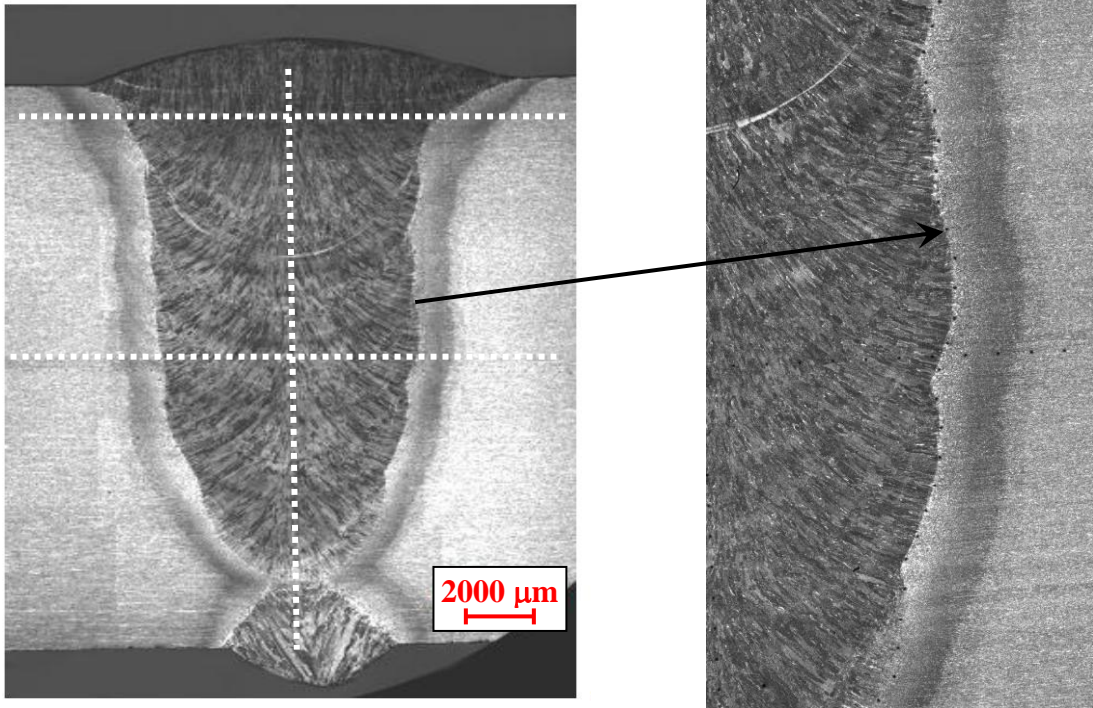


Figure 6. Macrograph of single torch X100 rolled pipe weld with vertical and horizontal lines indicating relative locations of through-thickness and cross-weld microhardness traverses. Enlarged image shows detail of through-thickness microhardness traverse in the coarse grain region adjacent to the fusion line.

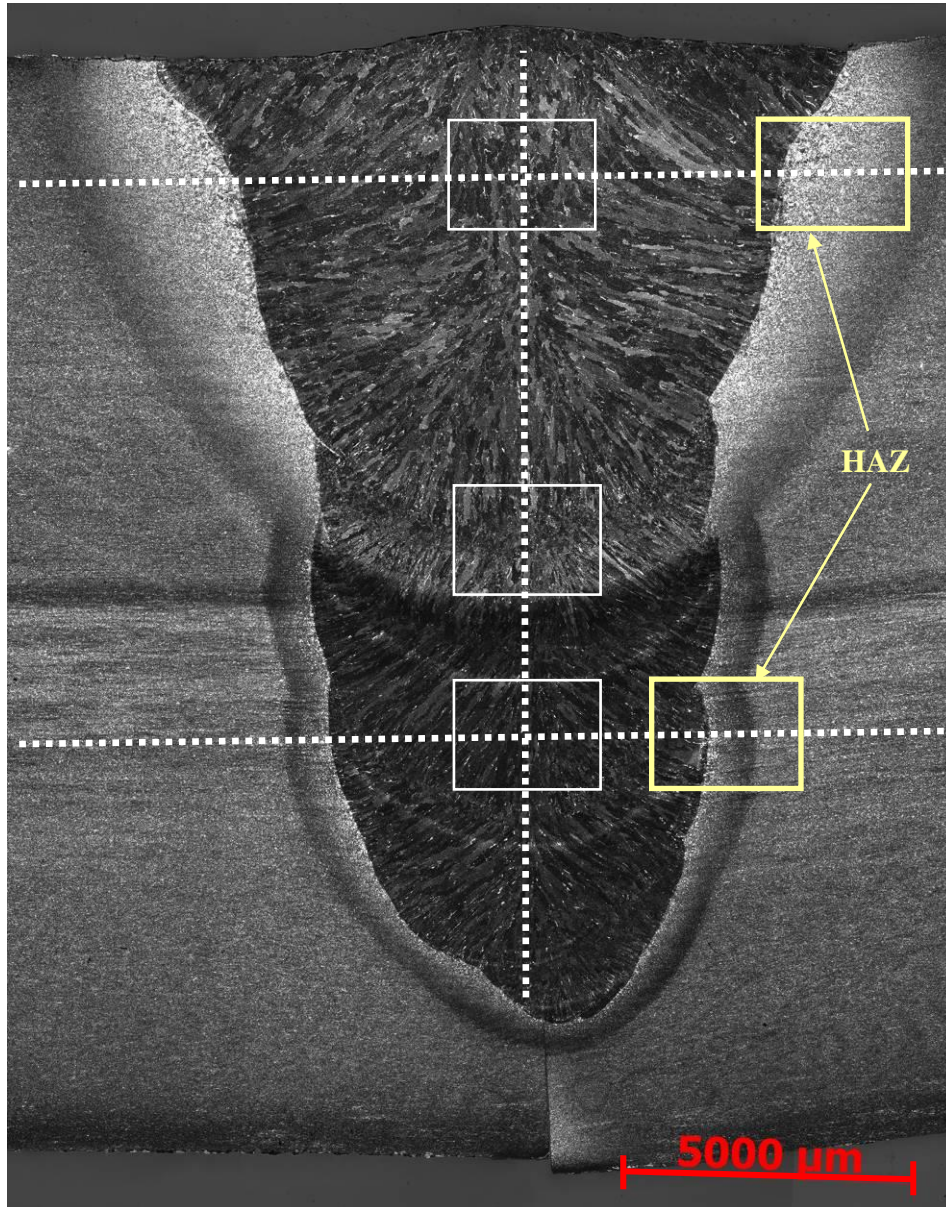
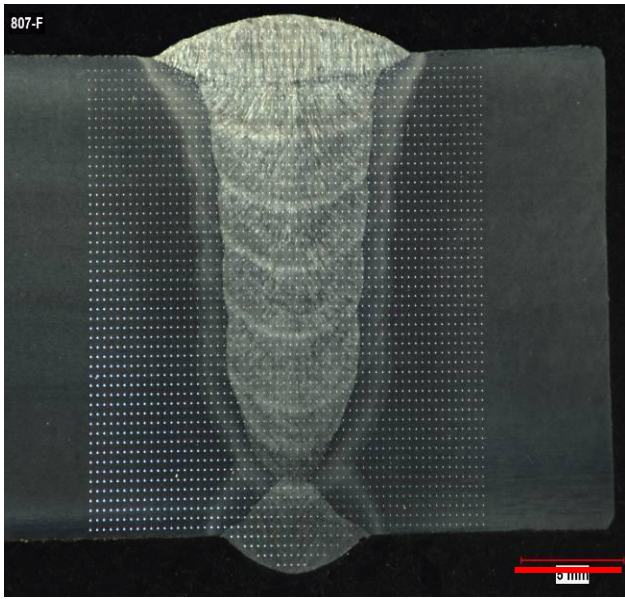
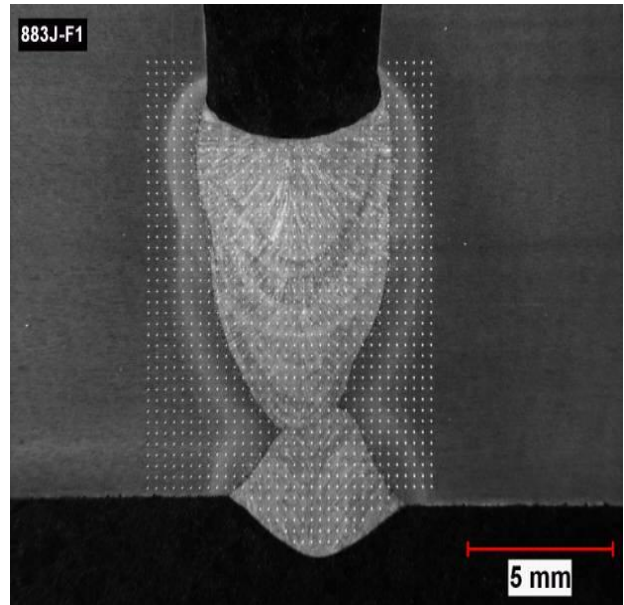


Figure 7. Macrograph of experimental weld showing areas (white rectangular boxes) used for characterization of as deposited and reheated WM microstructures and HAZ regions (yellow rectangular boxes). The vertical and horizontal dashed lines indicate the relative positions for the through-thickness and cross-weld microhardness surveys.

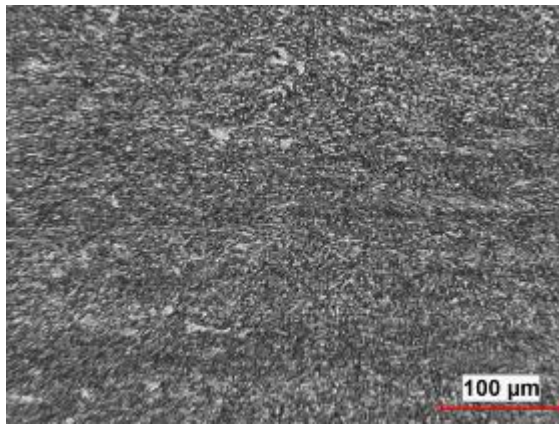


(a)

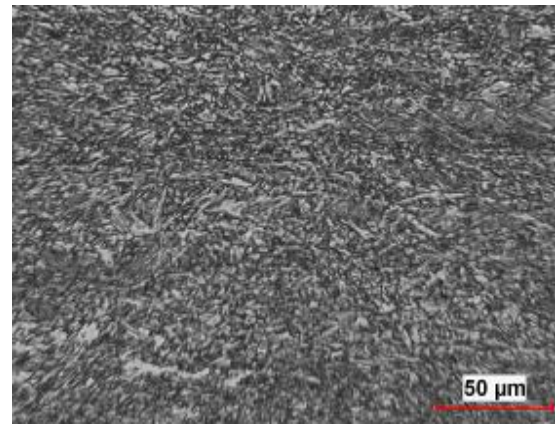


(b)

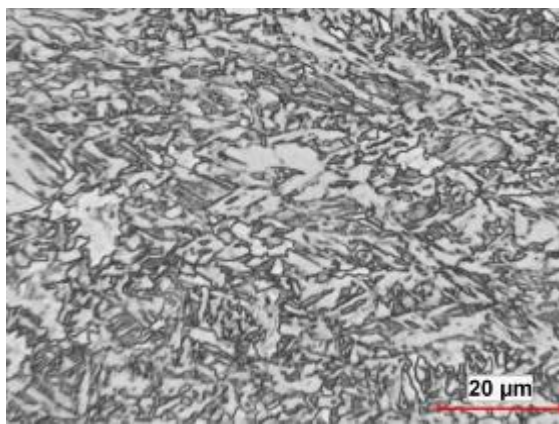
Figure 8. Macrographs showing hardness indent pattern used for (a) single torch and (b) staggered weld with root, hot and fill pass F1 completed.



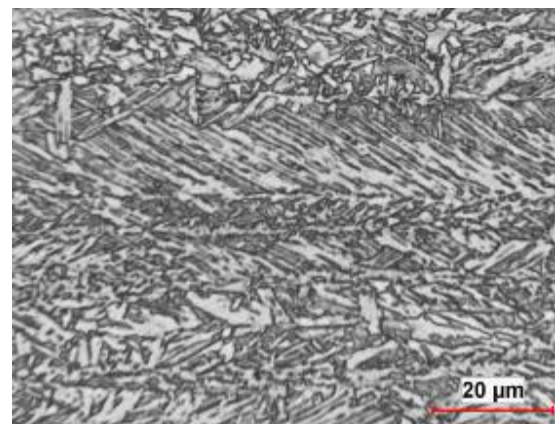
(a)



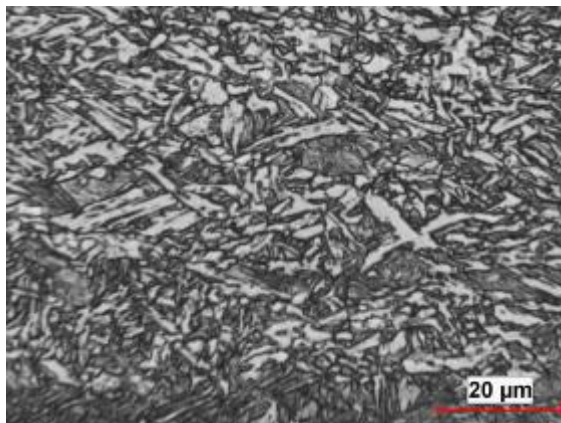
(b)



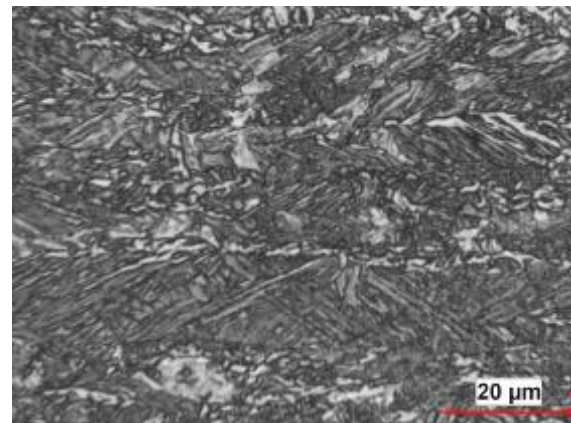
(c)



(d)



(e)



(f)

Figure 9. Optical micrographs of X100 pipe steel BM near the mid-wall for LPA orientation. (a, b) overall structure, (c, d) mainly bainite, and (e, f) higher proportions of martensite.

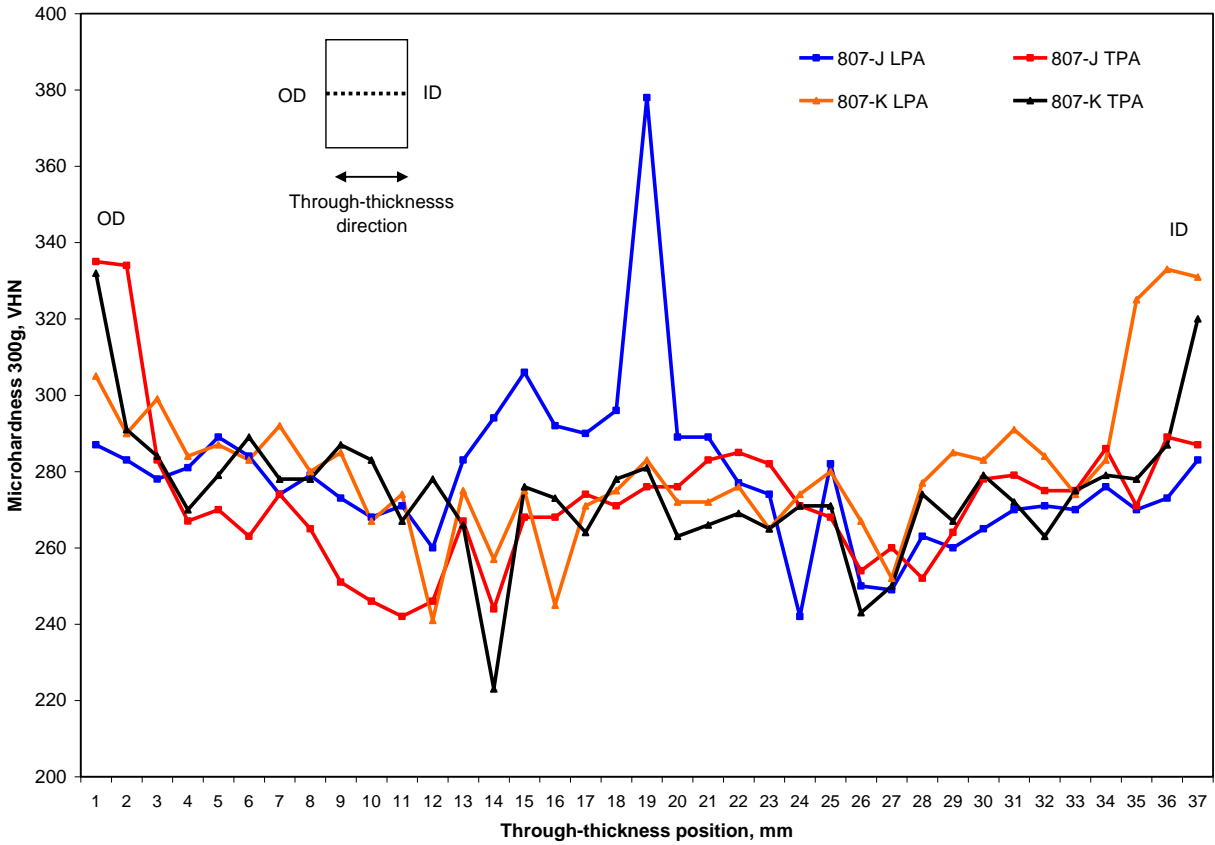


Figure 10. Through-thickness microhardness traverses for X100 pipe.

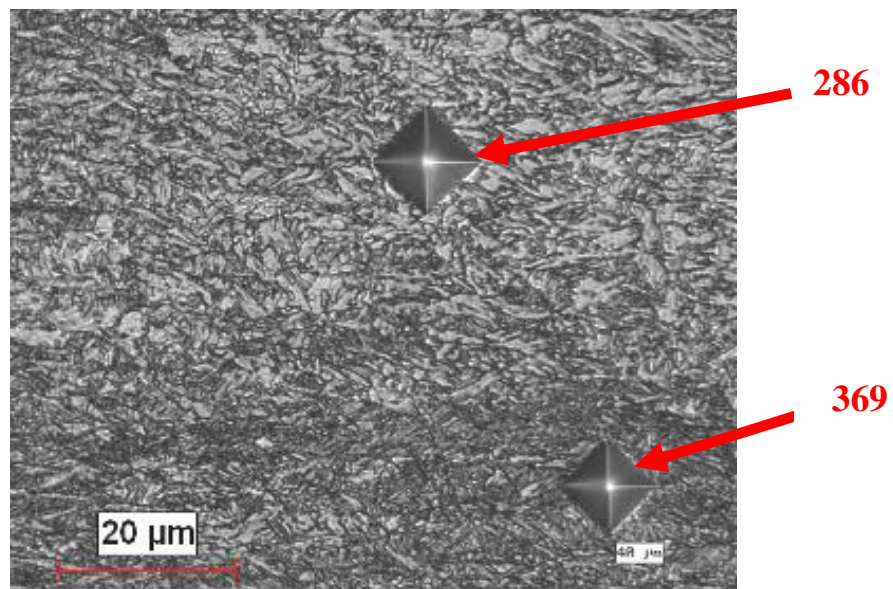


Figure 11. Optical micrograph showing hardness indents in mainly bainitic (286 VHN_{100g}) and predominantly martensitic (369 VHN_{100g}) regions.

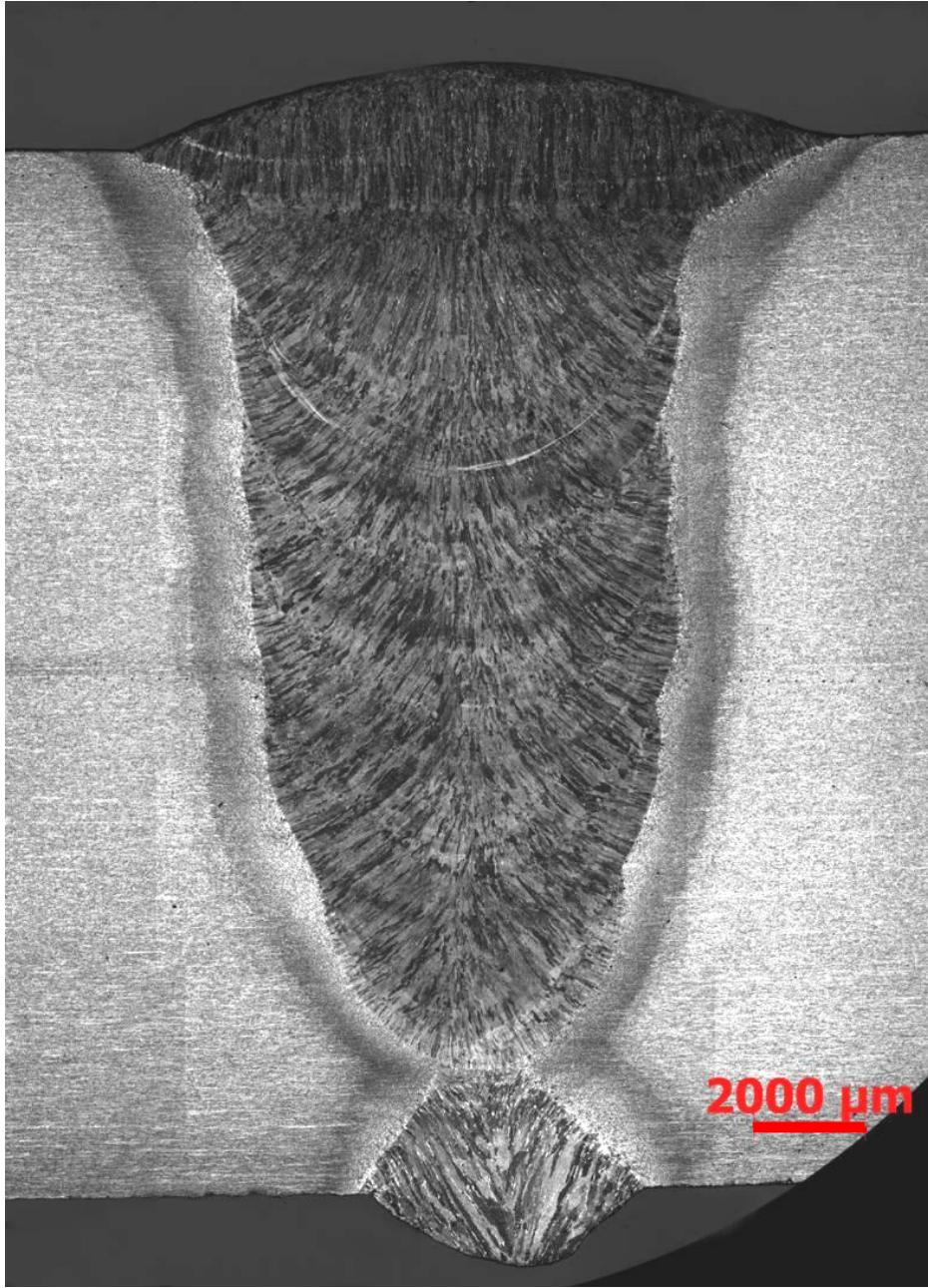


Figure 12. Representative macrograph of single torch X100 rolled pipe weld 807F.

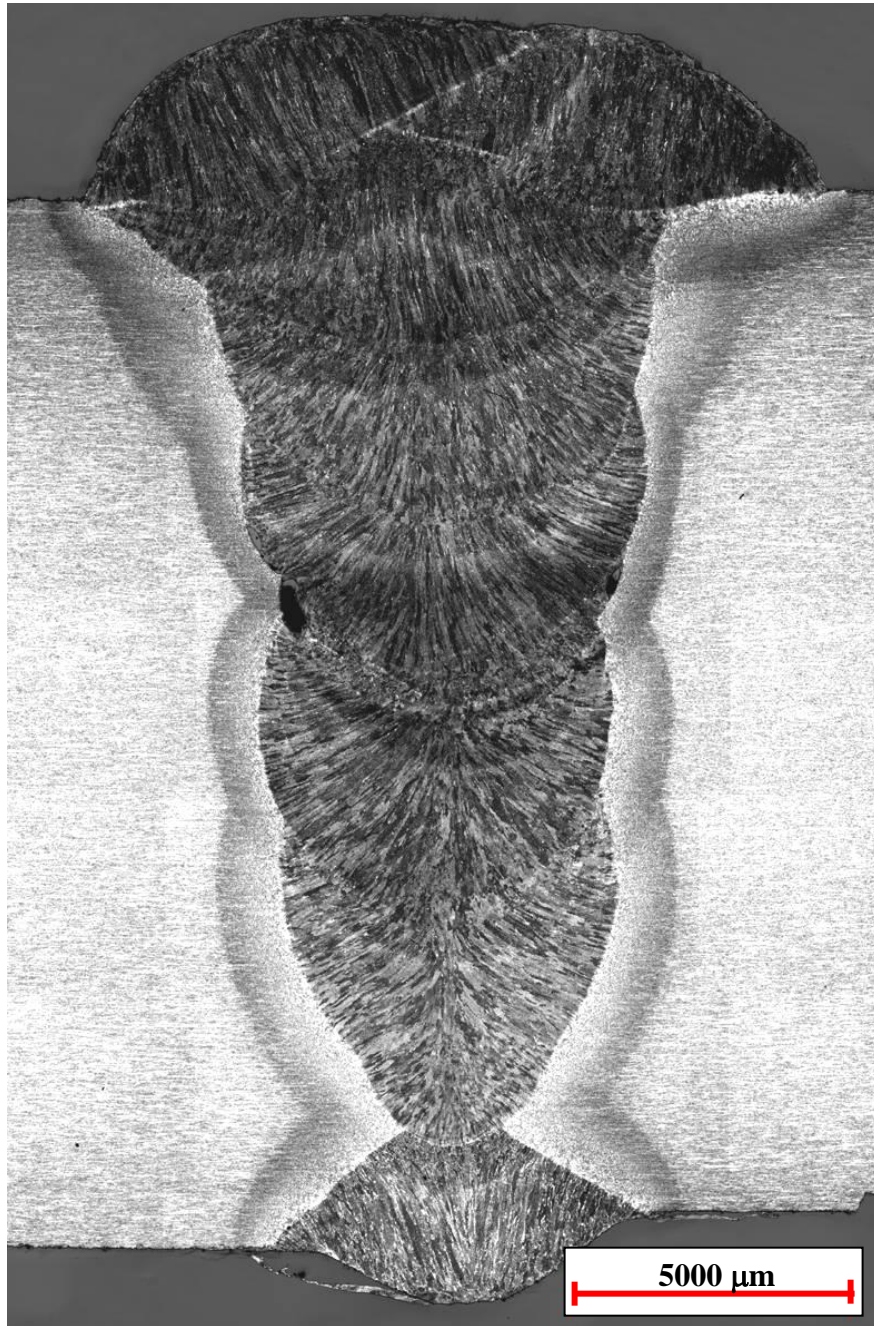
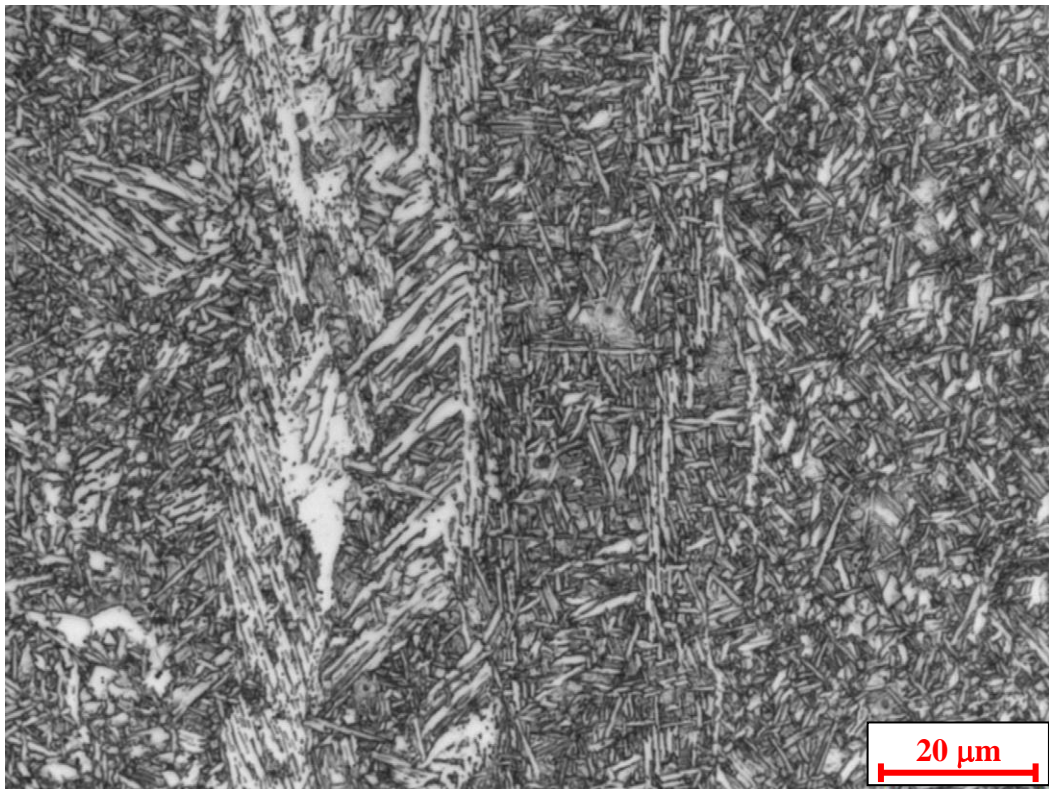
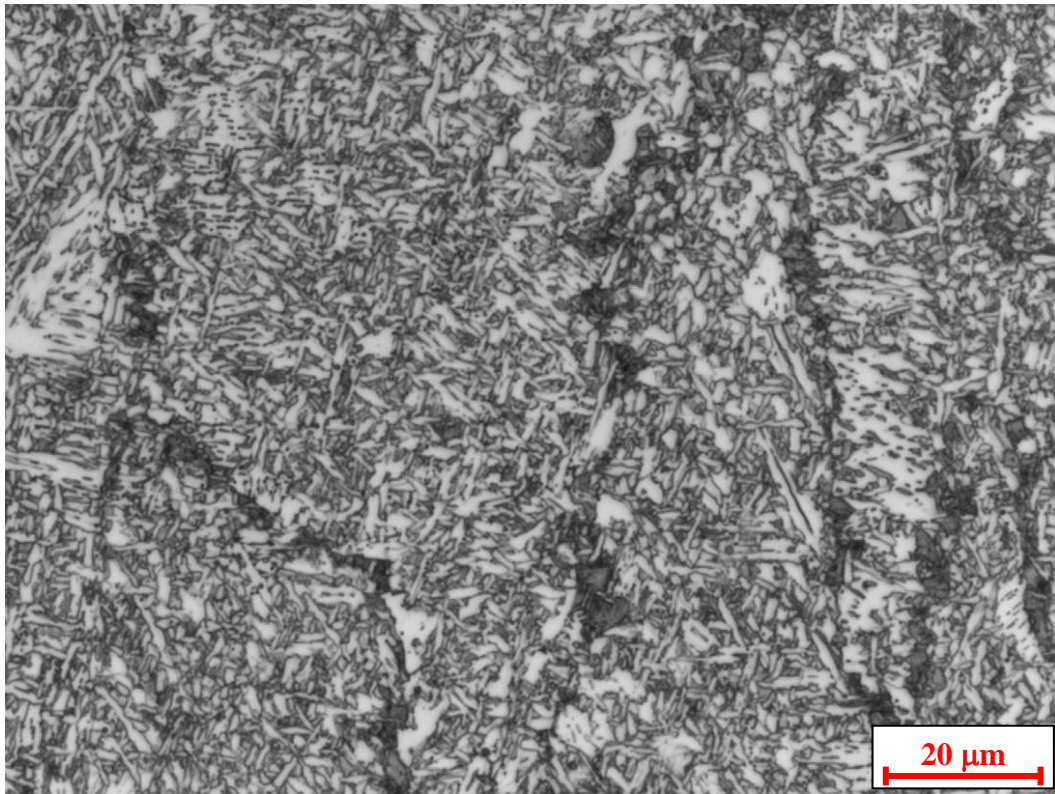


Figure 13. Representative macrograph of dual torch X100 rolled pipe weld 883D.

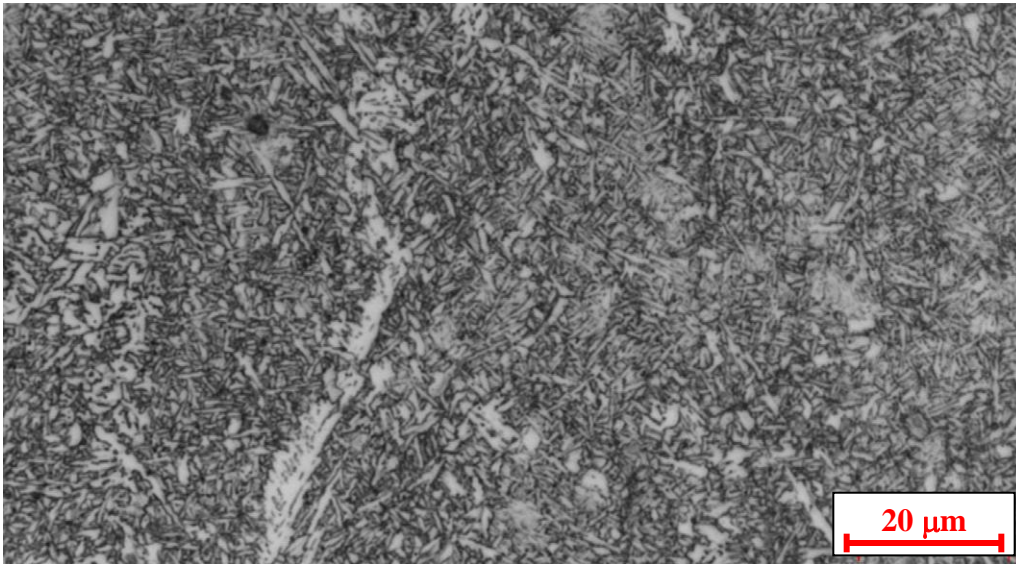


(a) As-deposited WM of cap pass

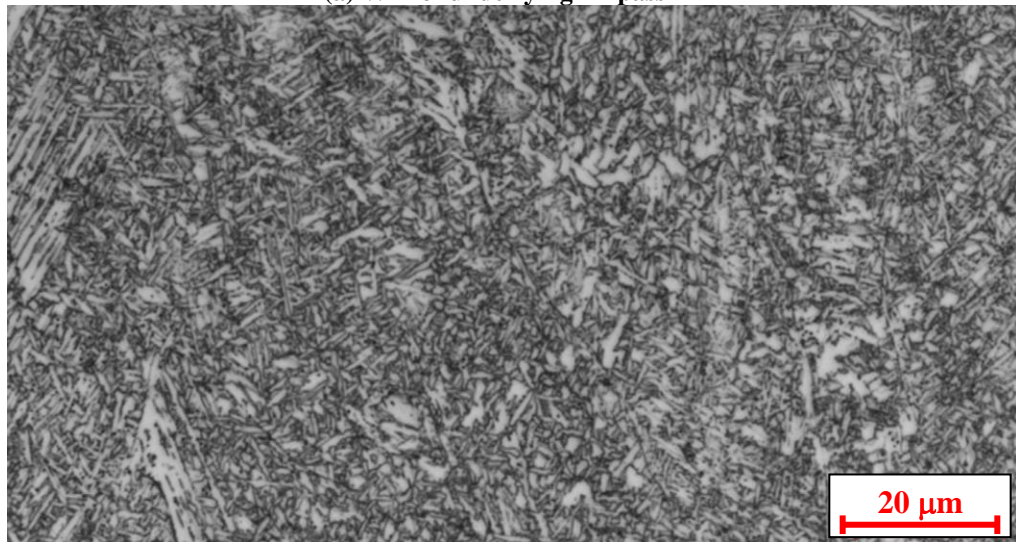


(b) Reheated WM beneath cap pass

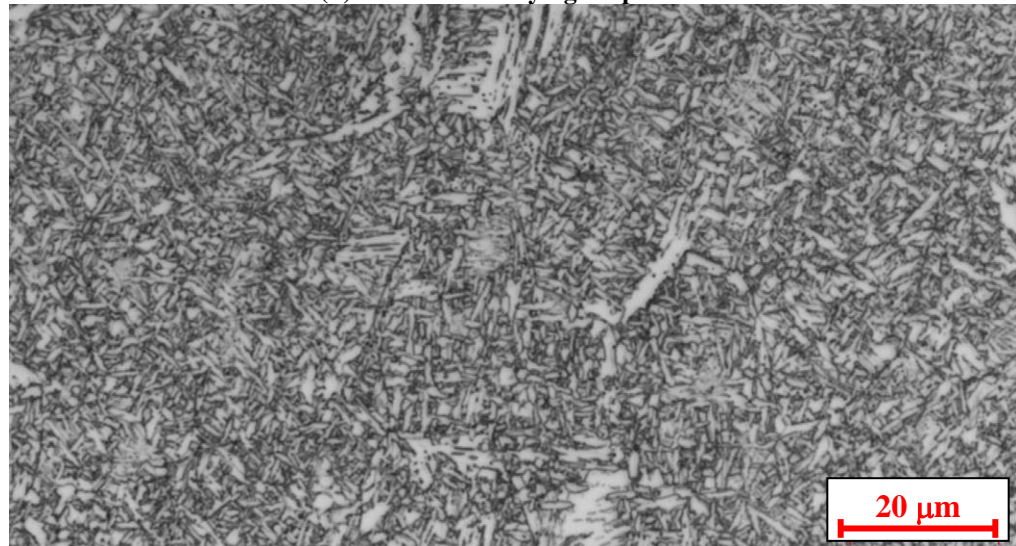
Figure 14. WM microstructures of the cap pass in single torch weld 807J.



(a) WM of underlying fill pass F4

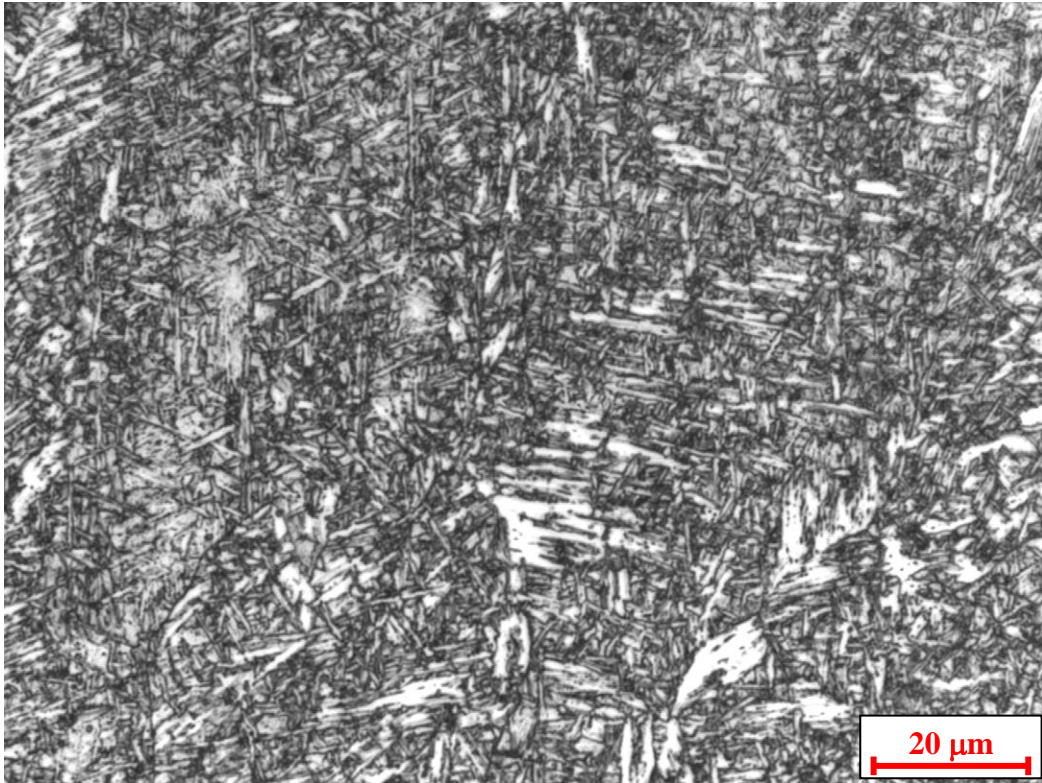


(b) WM of underlying fill pass F3

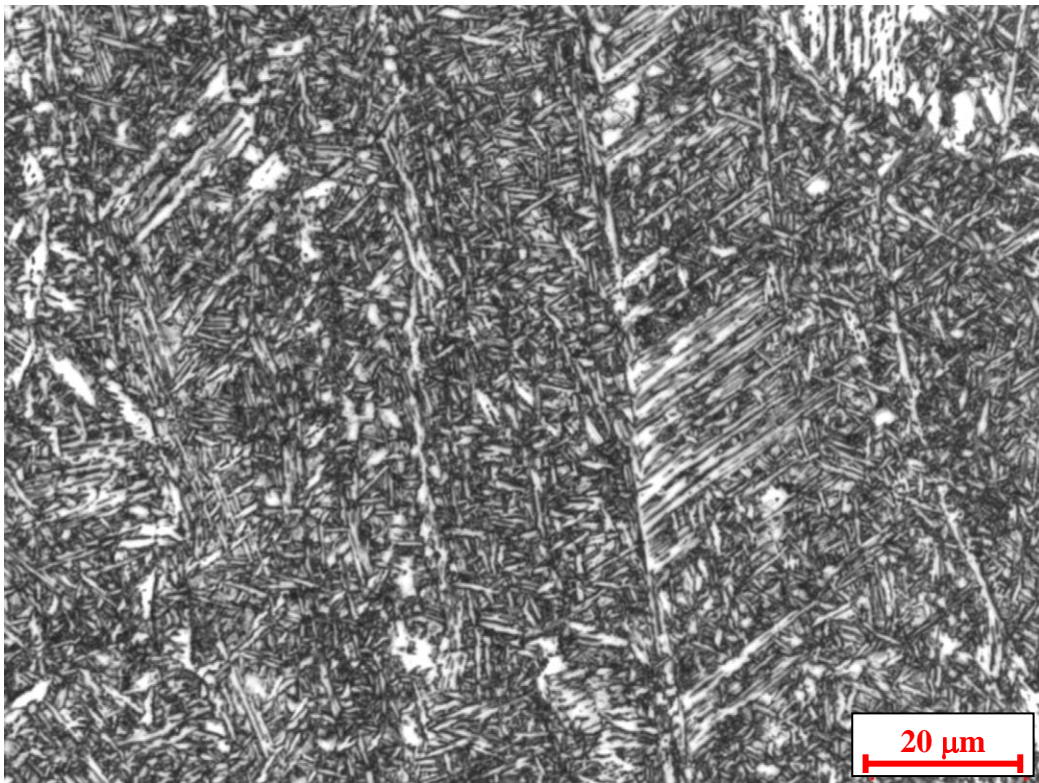


(c) WM of underlying fill pass F2

Figure 15. WM microstructures in underlying fill passes of single torch weld 807J.

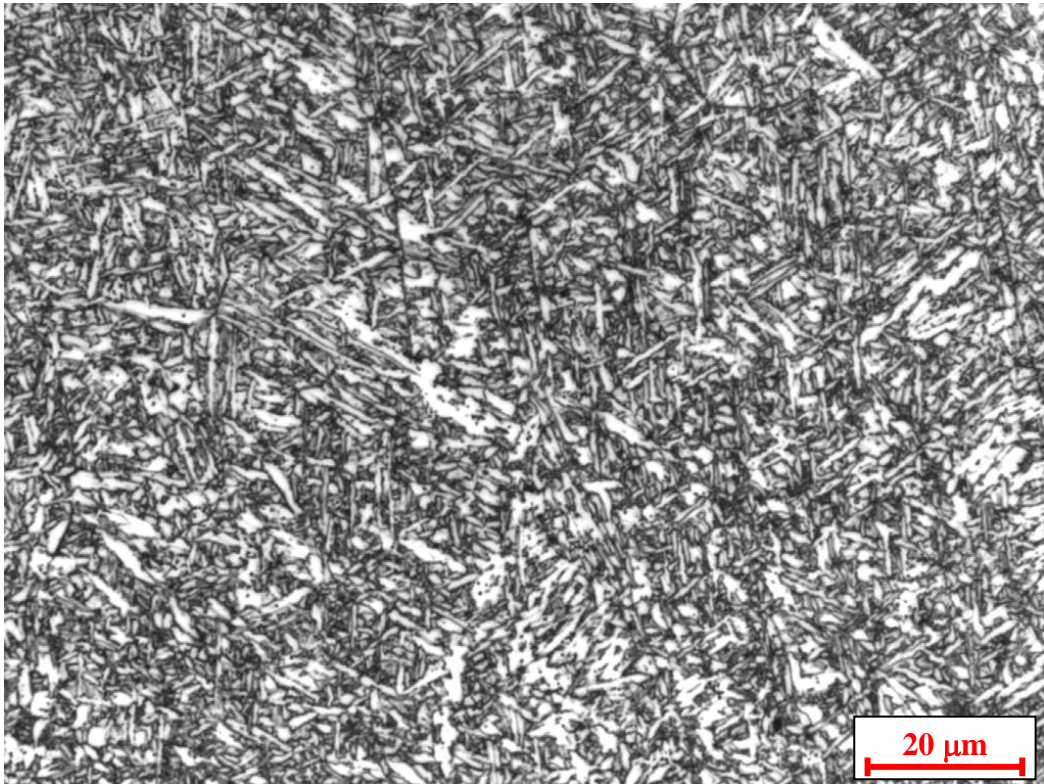


(a) As-deposited WM of cap pass 2 (trail wire).

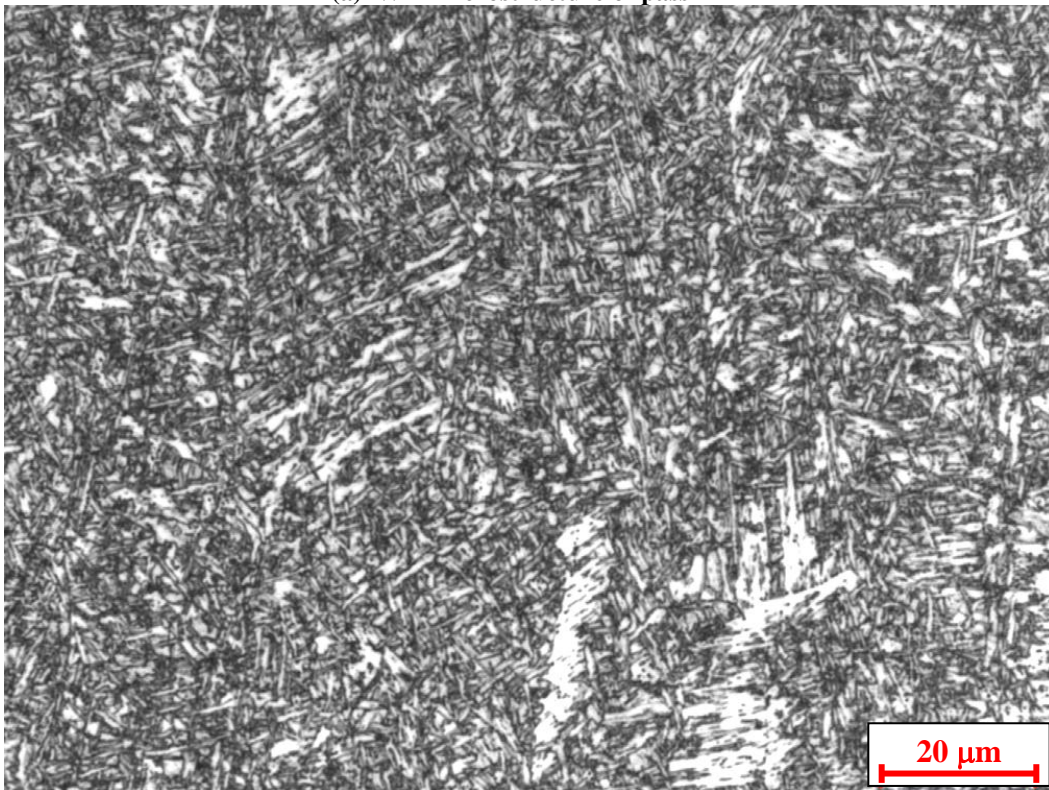


(b) As-deposited WM of cap pass 1 (lead wire).

Figure 16. WM microstructures of the split cap passes for dual torch weld 883D.

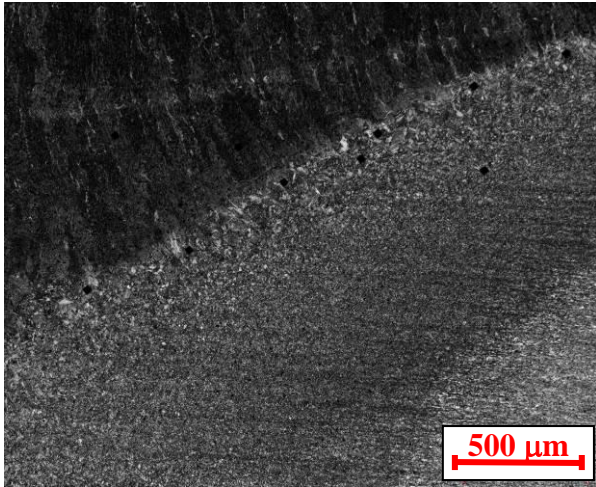


(a) WM microstructure of pass D4

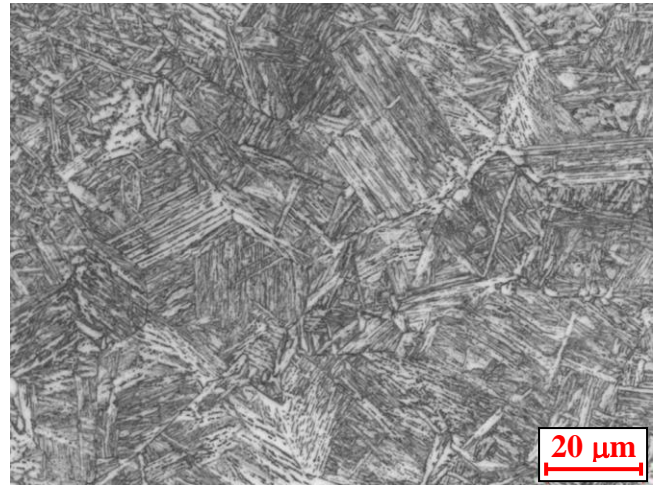


(b) WM microstructure of pass D3

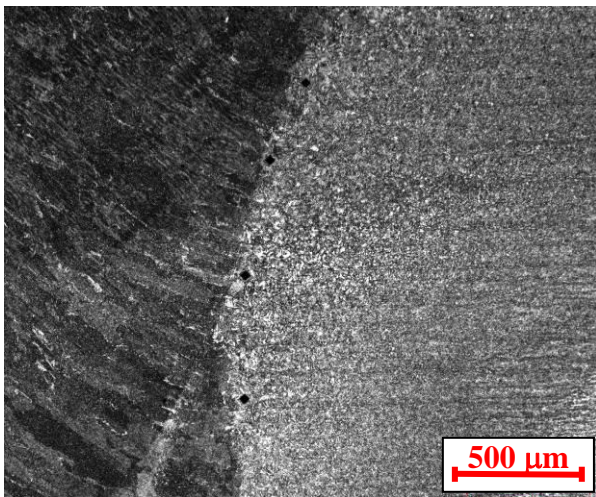
Figure 17: WM microstructure of dual torch pass D4 and the underlying pass D3.



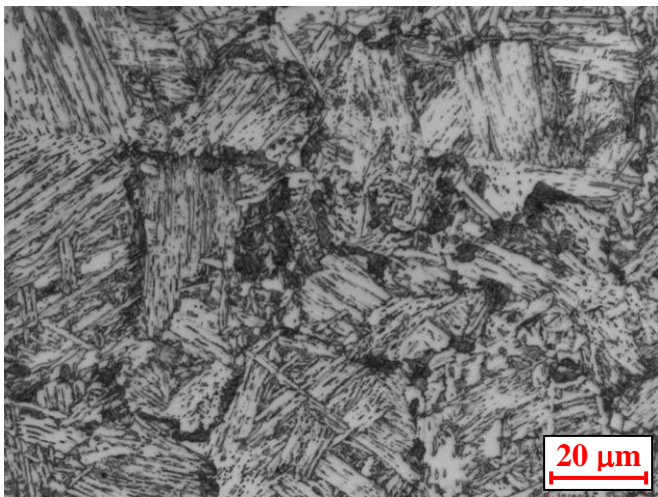
(a) HAZ region near the cap pass



(b) GCHAZ microstructure near the cap pass

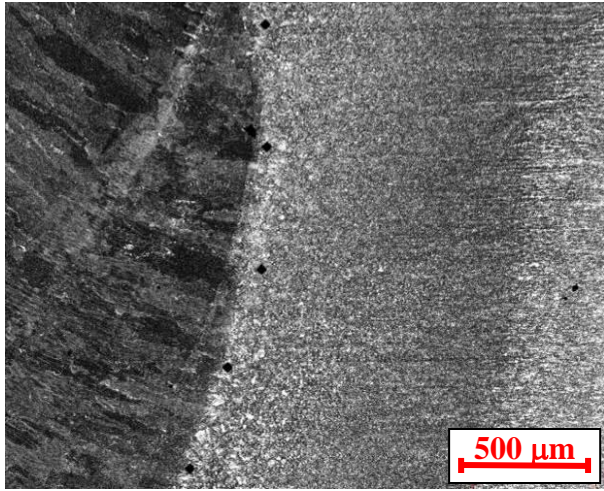


(c) HAZ region near bottom of cap pass

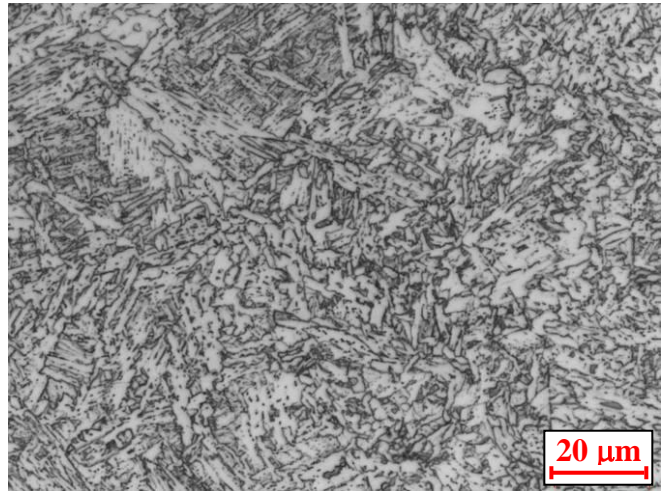


(d) ICR-GCHAZ microstructure near cap pass

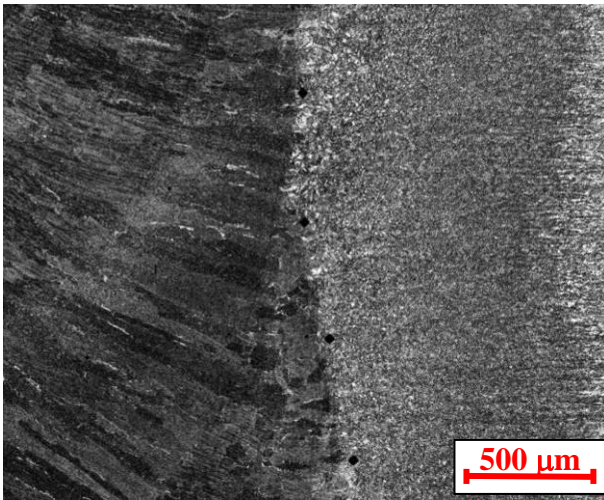
Figure 18. HAZ microstructures of the single torch weld 807-J.



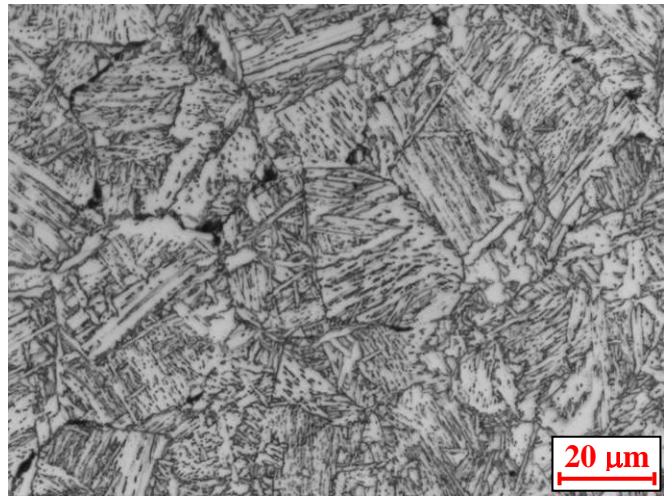
(a) HAZ region near fill pass F4



(b) Reheated GCHAZ structure near fill pass F4

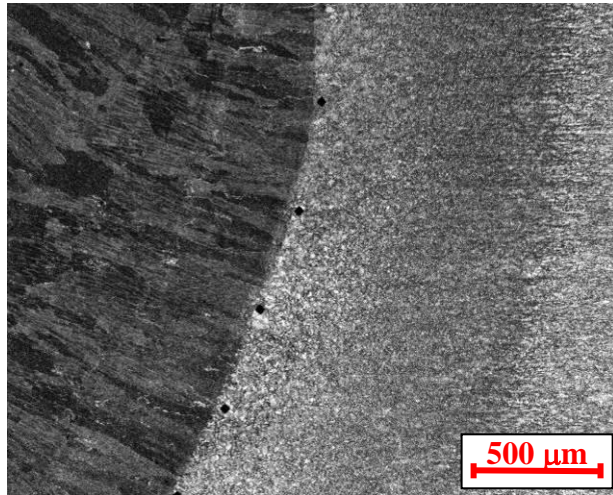


(c) HAZ microstructure near fill pass F4

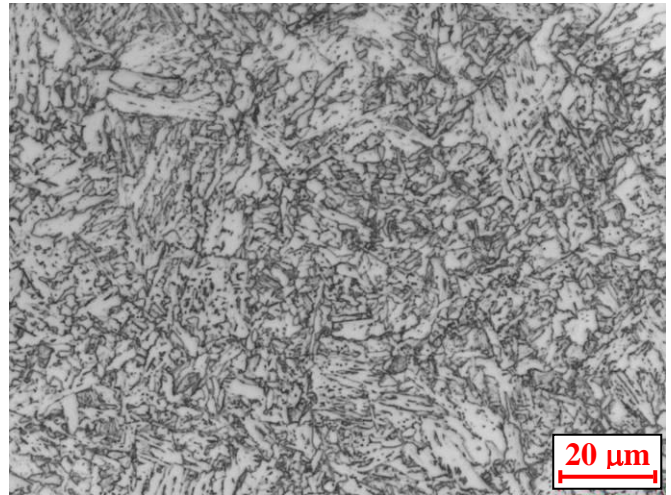


(d) ICR-GCHAZ microstructure near fill pass F4

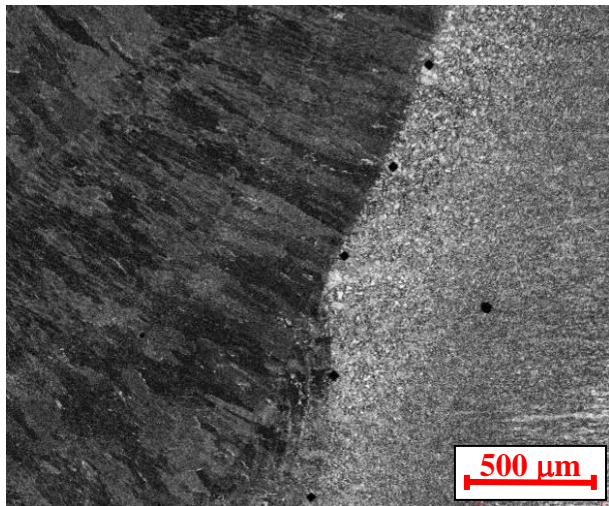
Figure 19. HAZ microstructures of the single torch weld 807-J.



(a) HAZ region near fill pass F2



(b) Reheated GHAZ structure near fill pass F2

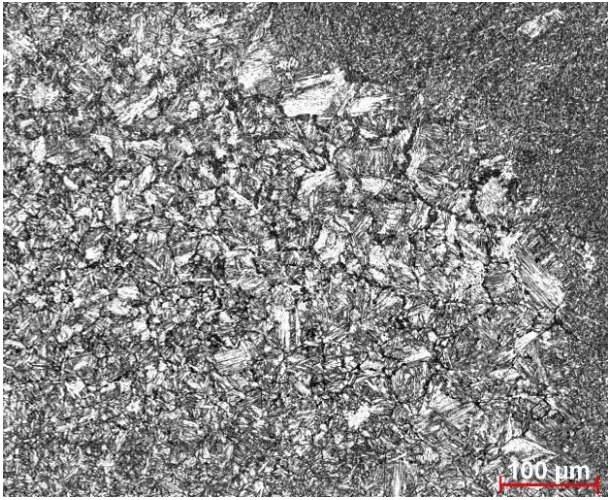


(c) HAZ microstructure near fill pass F2

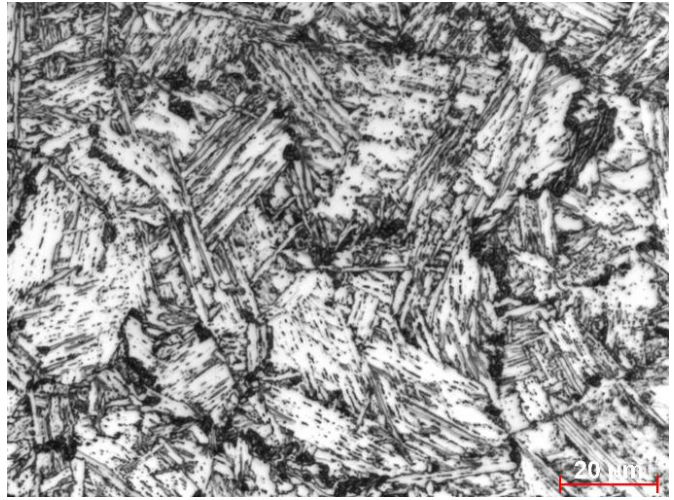


(d) HAZ microstructure near fill pass F2

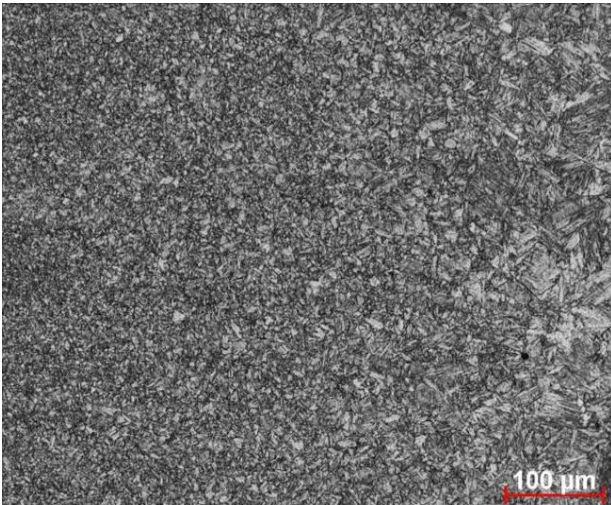
Figure 20. HAZ microstructures of the single torch weld 807-J.



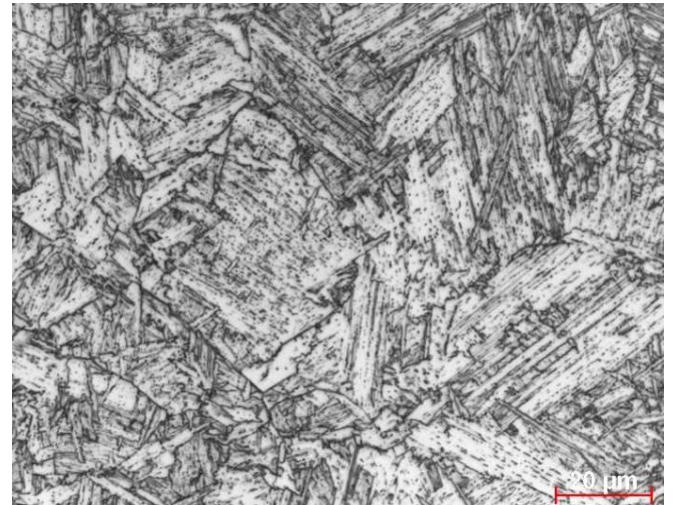
(a) HAZ region near cap pass



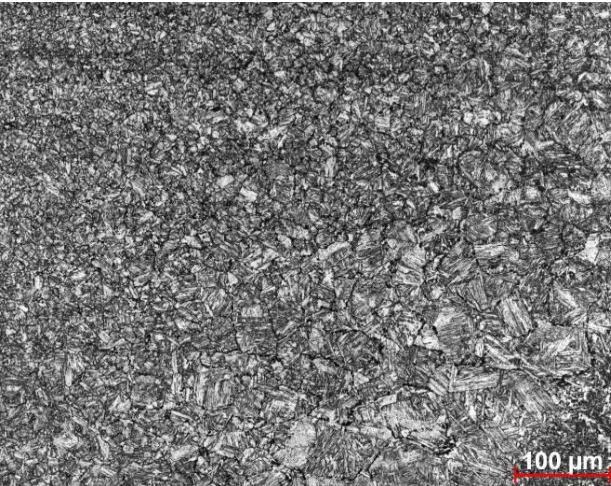
(b) ICR-GCHAZ structure near cap



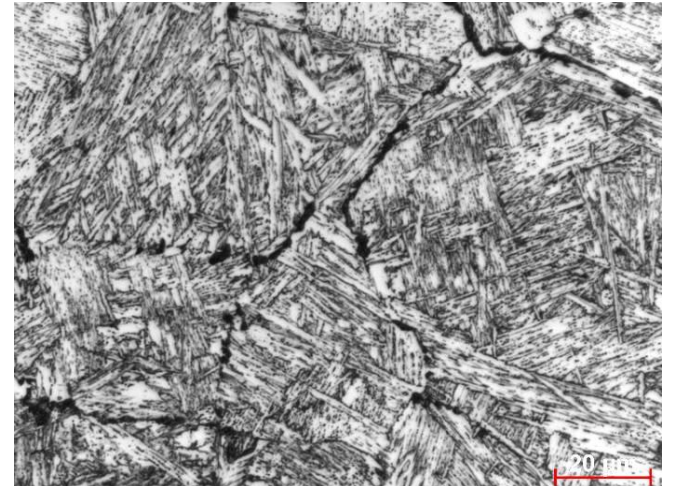
(c) HAZ region near mid-wall



(d) HAZ microstructure near mid-wall

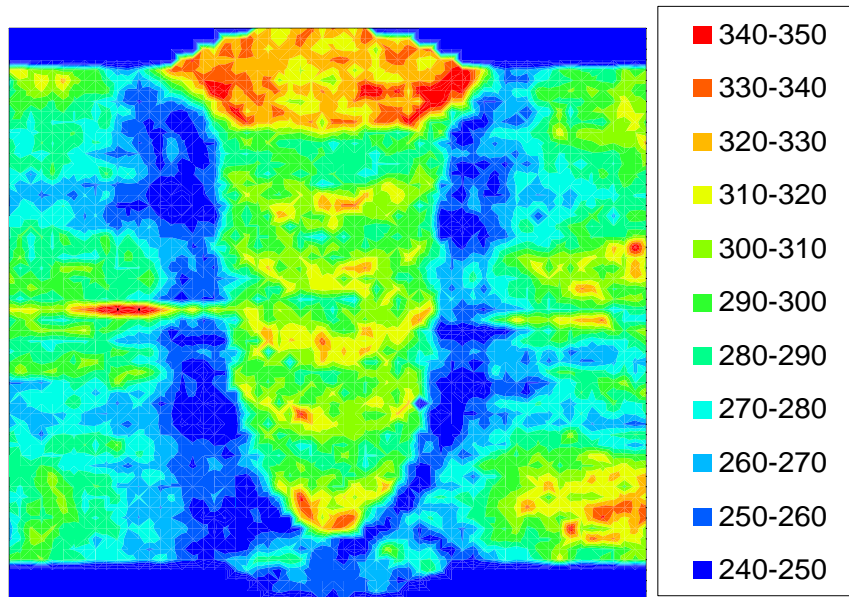


(e) HAZ region near root pass

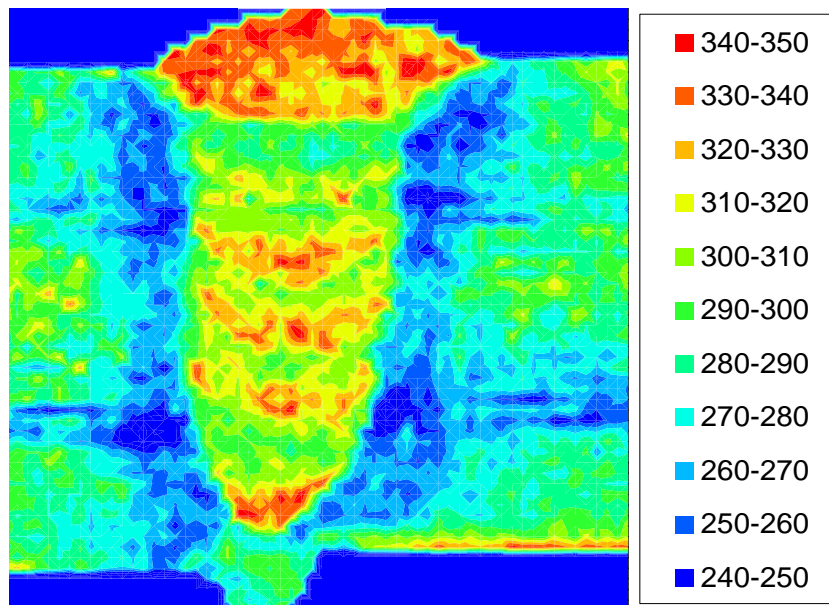


(f) HAZ region near root pass

Figure 21. HAZ microstructures formed in the dual torch weld 883-D.

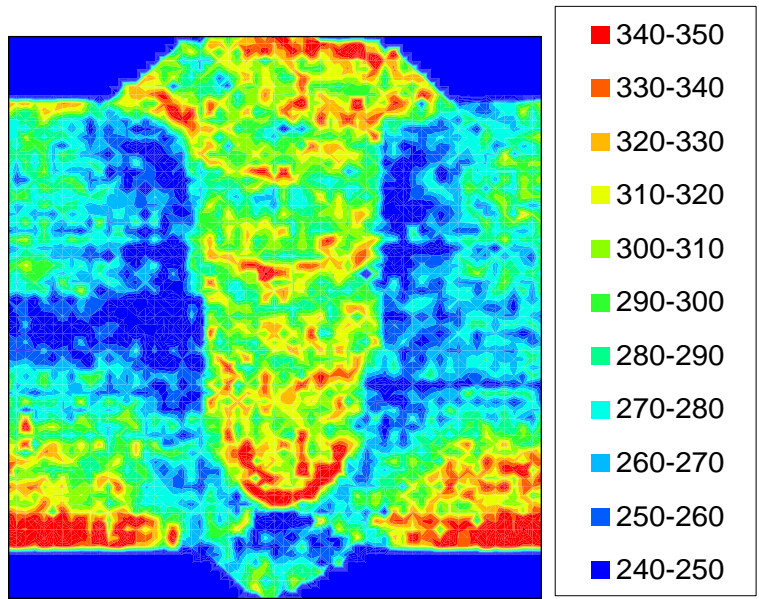


(a) 807-J

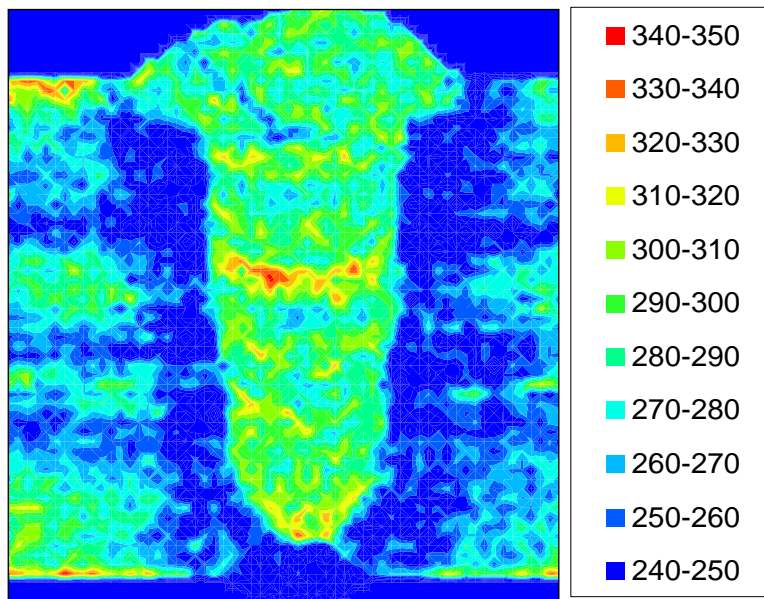


(b) 807-K

Figure 22. Microhardness maps for selected single torch pipe welds. Scale units = VHN₃₀₀



(a) 883-D



(b) 883-F

Figure 23. Microhardness maps for selected dual torch pipe welds. Scale units = VHN₃₀₀

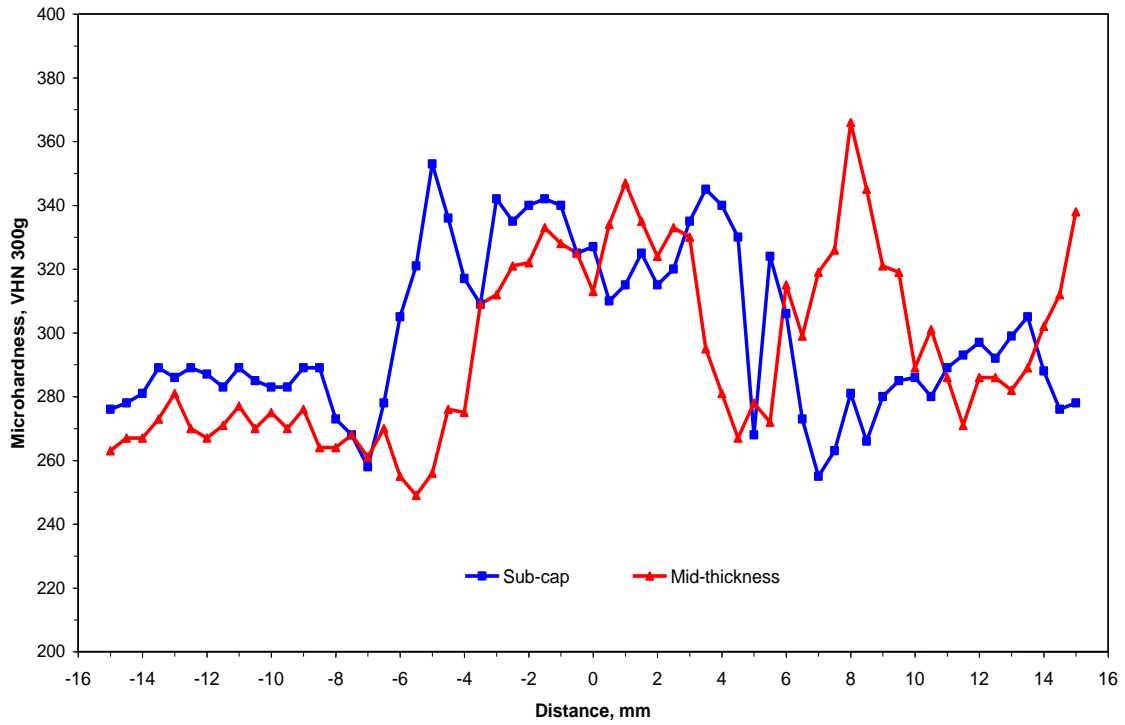


Figure 24. Cross-weld microhardness traverses for single torch pipe weld, 807-J.

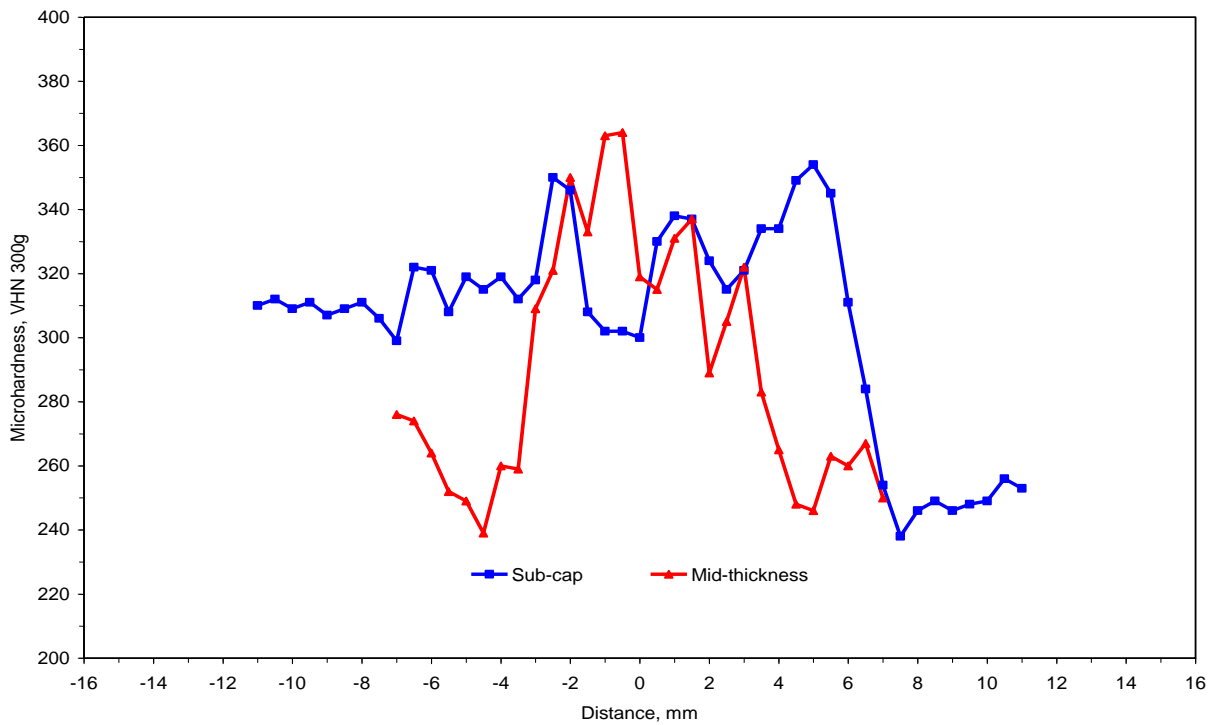


Figure 25. Cross-weld microhardness traverses for dual torch pipe weld, 883-D.

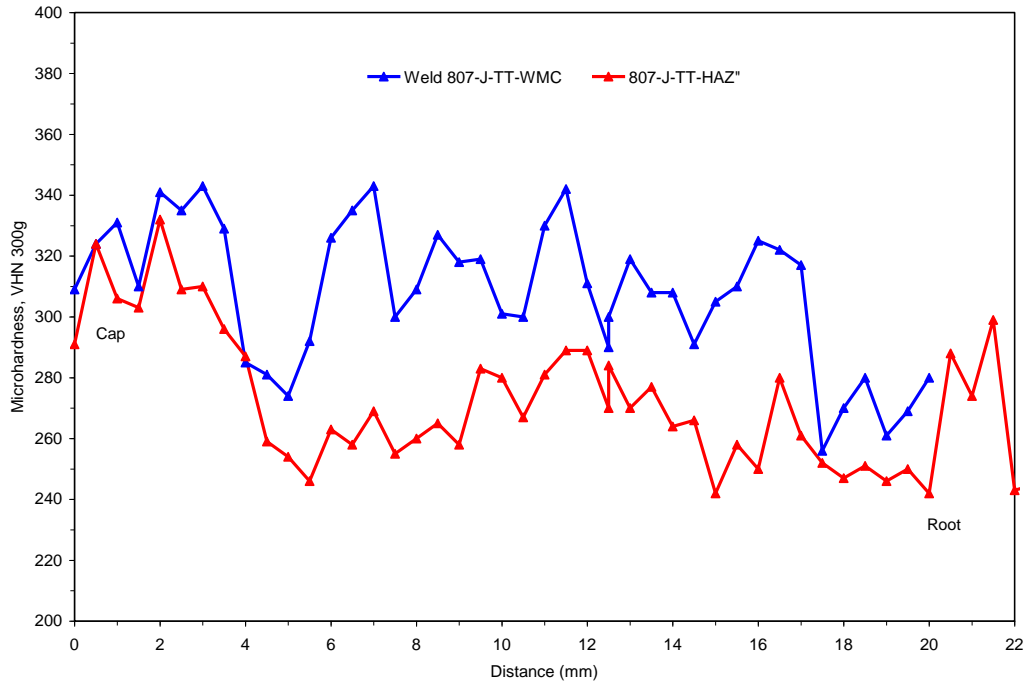


Figure 26. Through-thickness microhardness traverses for single torch pipe weld, 807-J.

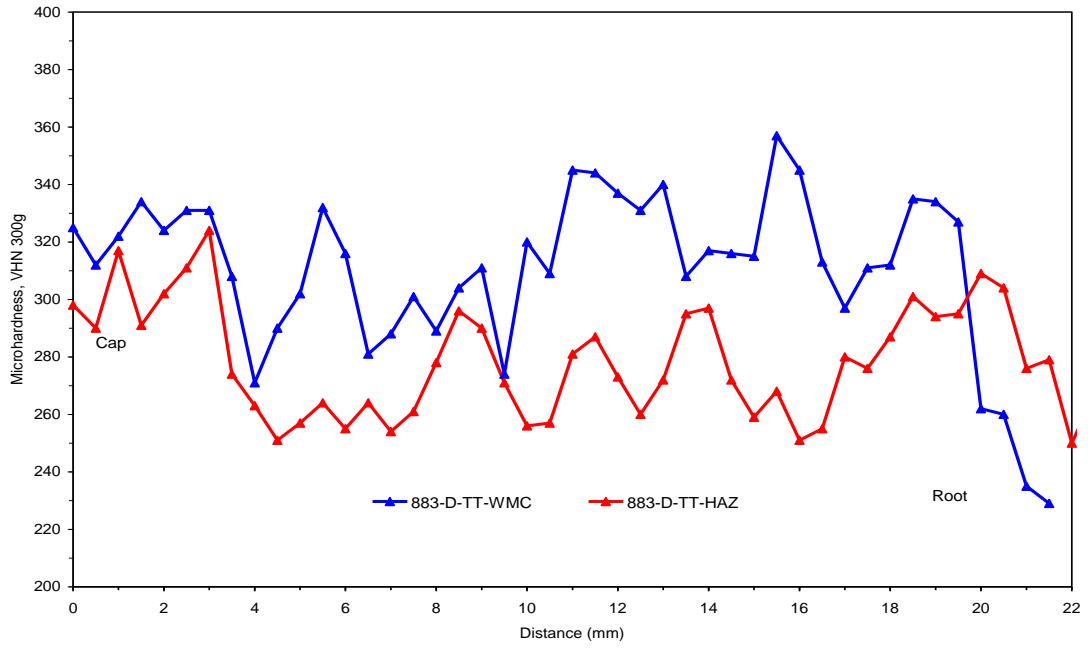


Figure 27. Through-thickness microhardness traverses for single torch pipe weld, 883-D.

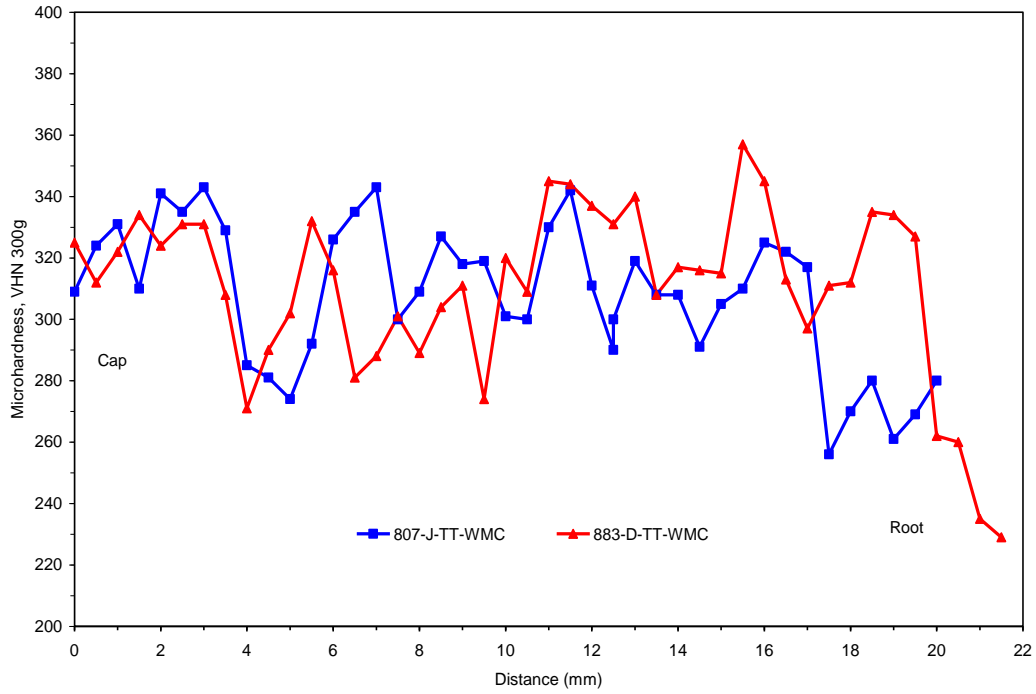


Figure 28. Comparison of through-thickness WMC microhardness traverses.

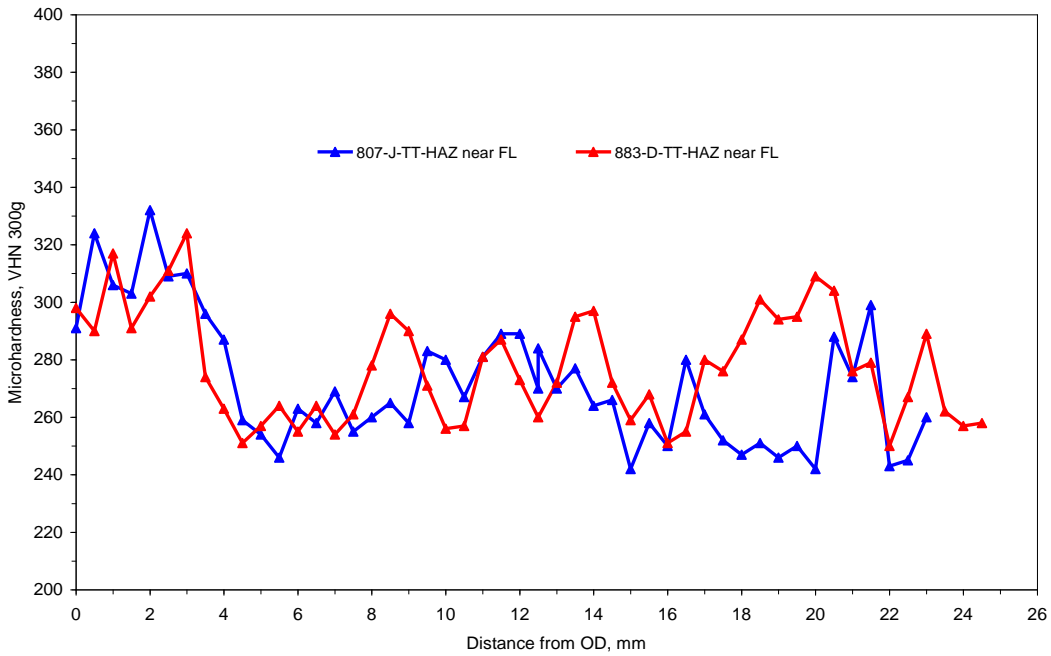


Figure 29. Comparison of through-thickness HAZ microhardness traverses.

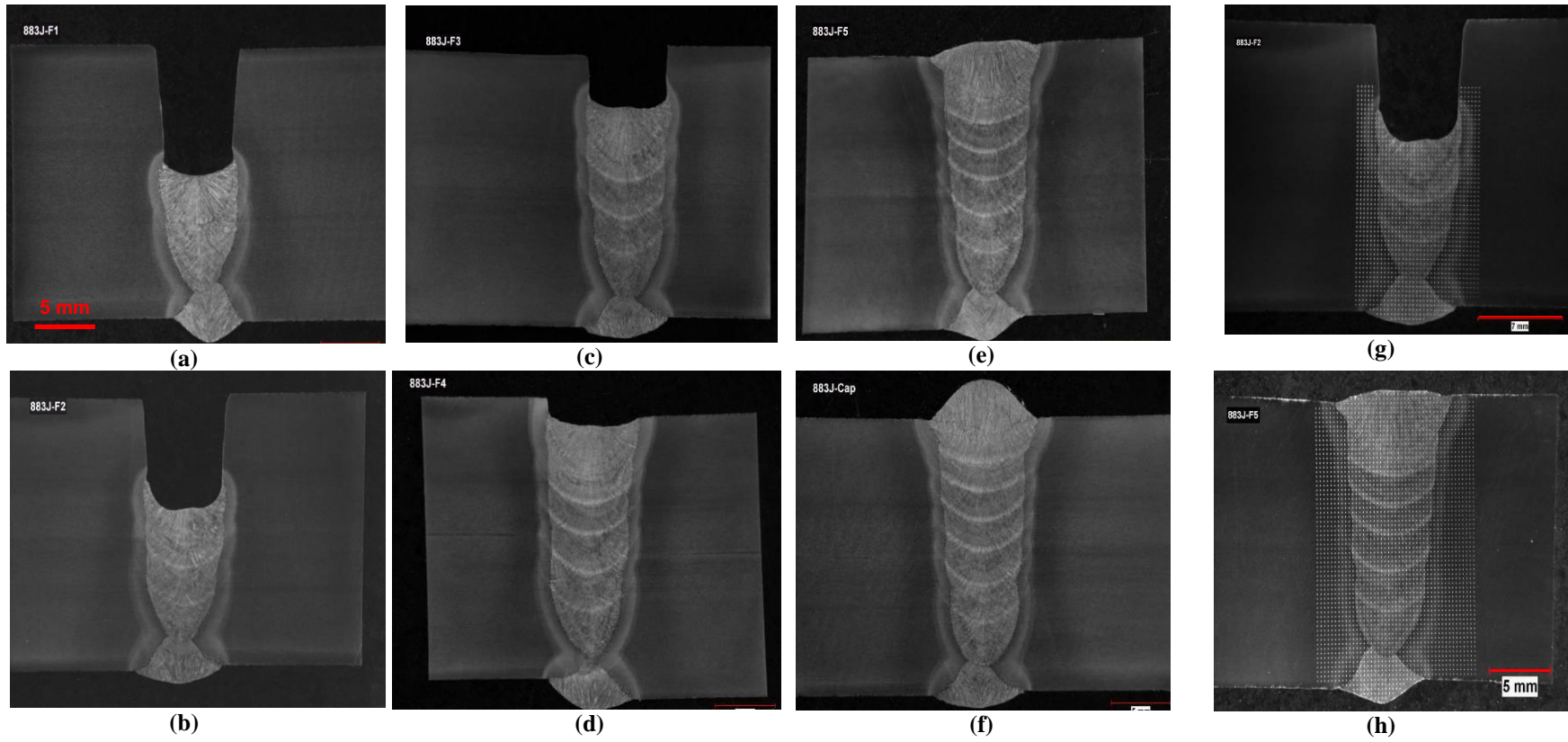
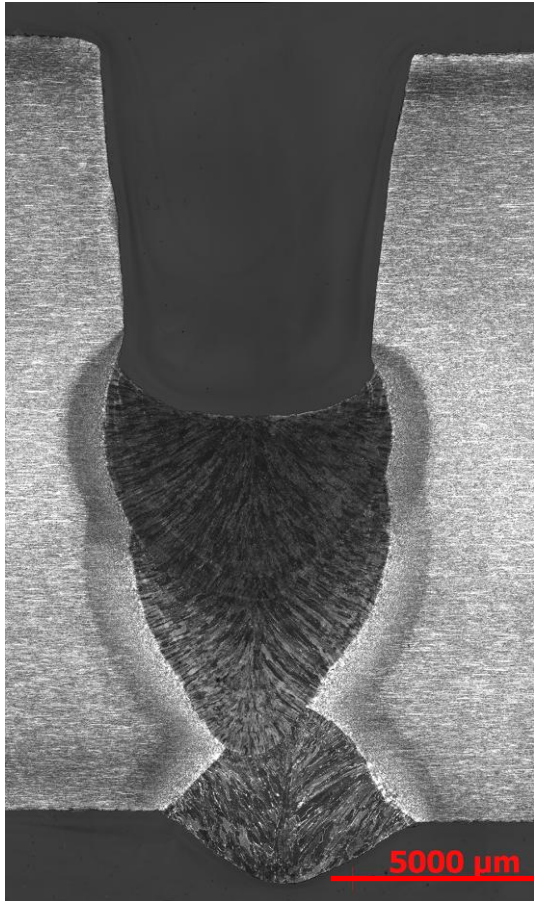


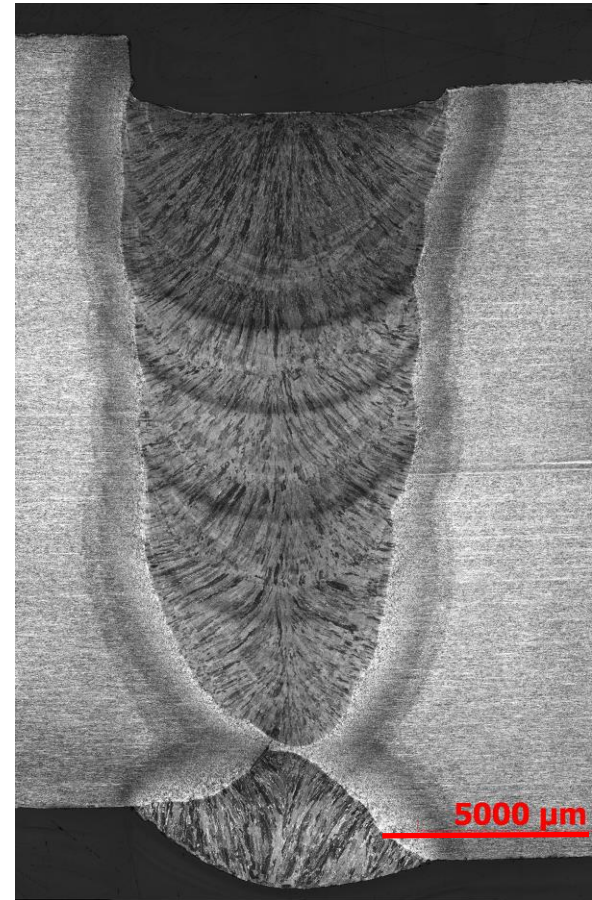
Figure 30. Macrographs showing (a-f) staggered fill and cap passes in single torch X100 rolled weld, 883J and (g, h) microhardness mapping indent patterns. Pipe wall thickness = 19 mm.



Fill pass F1



Fill pass F2



Fill pass F4

Figure 31. Detail of staggered fill passes of single torch X100 rolled weld, 883J. Pipe wall thickness = 19 mm

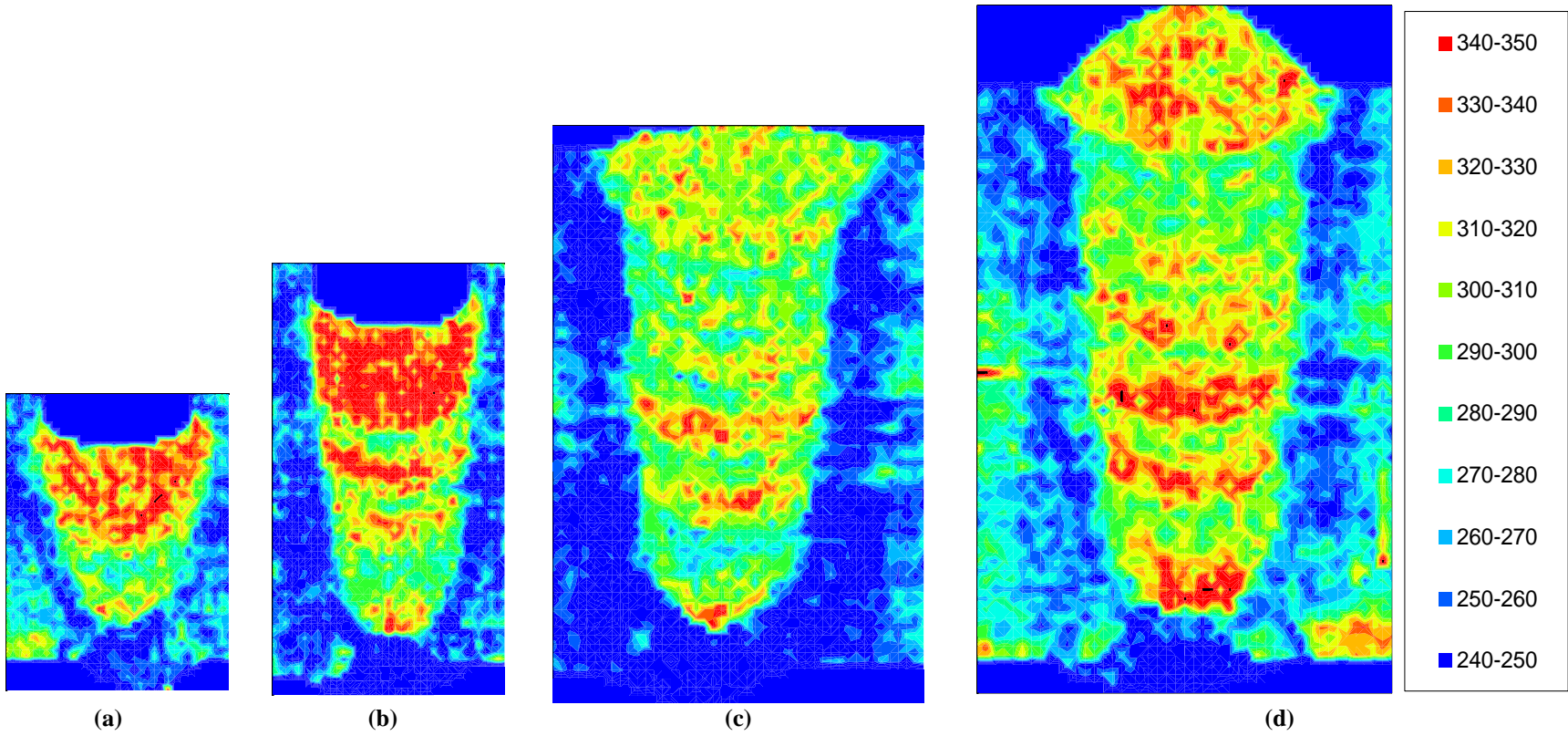


Figure 32. Microhardness maps of staggered fill passes (a) F1, (b) F3, (c) F5, and (d) completed weld with cap pass for single torch X100 rolled weld 883J.

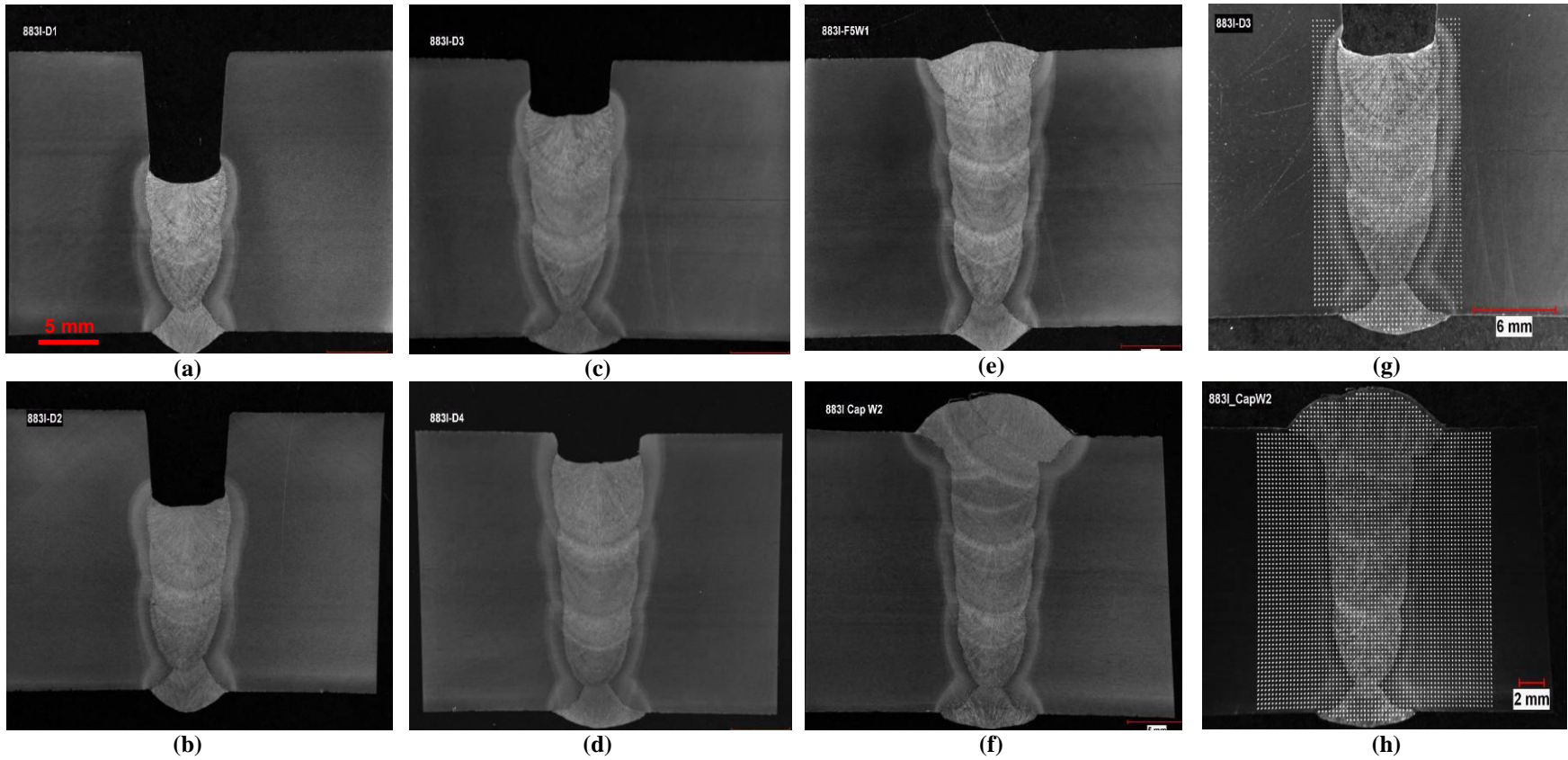
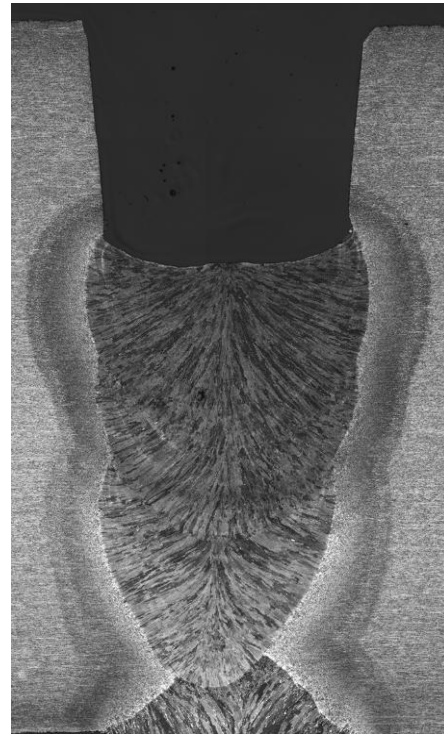


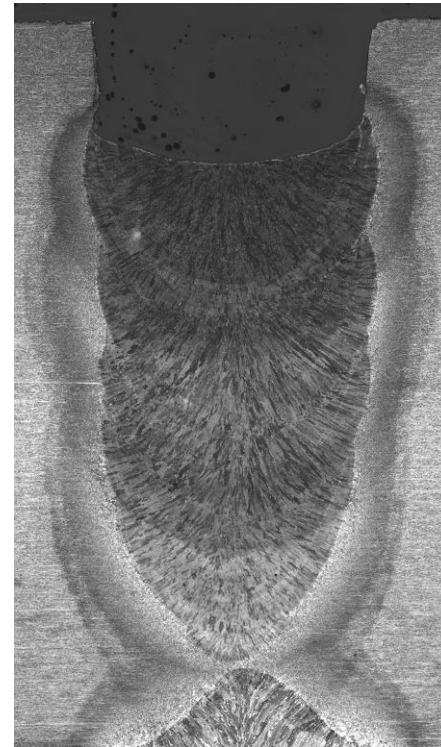
Figure 33. Macrographs showing (a-f) staggered fill and cap passes in dual torch X100 rolled weld, 883I and (g, h) microhardness mapping indent patterns. Pipe wall thickness = 19 mm



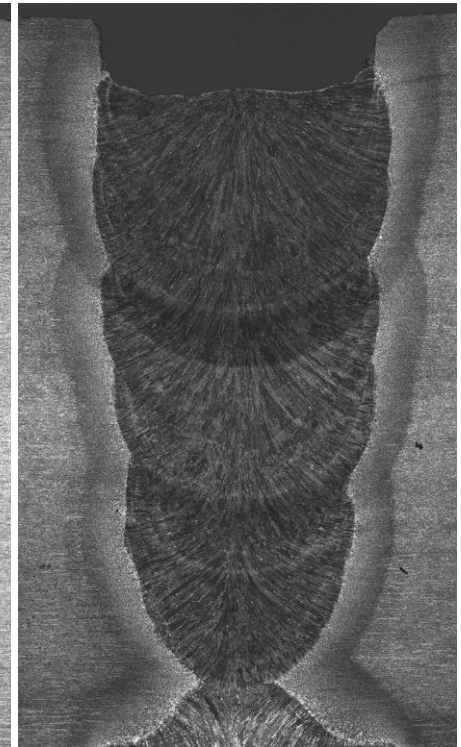
Fill pass D1



Fill pass D2



Fill pass D3



Fill pass D3

Figure 34. Detail of staggered fill passes in dual torch X100 rolled weld, 883I. Pipe wall thickness = 19 mm

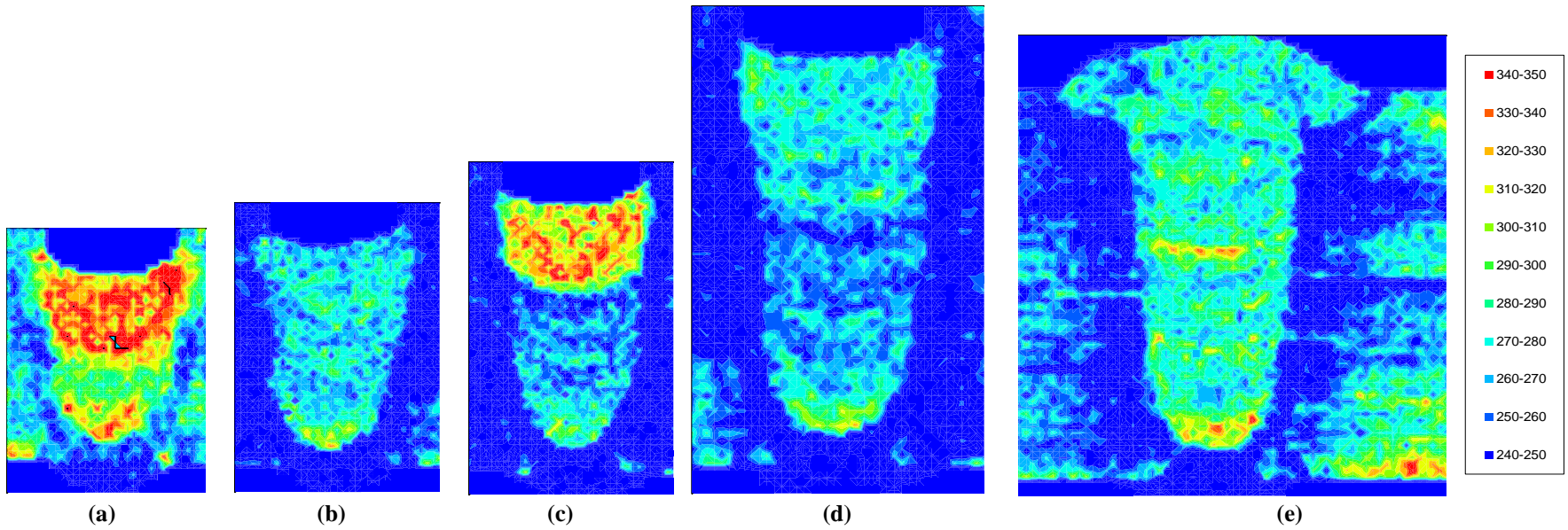
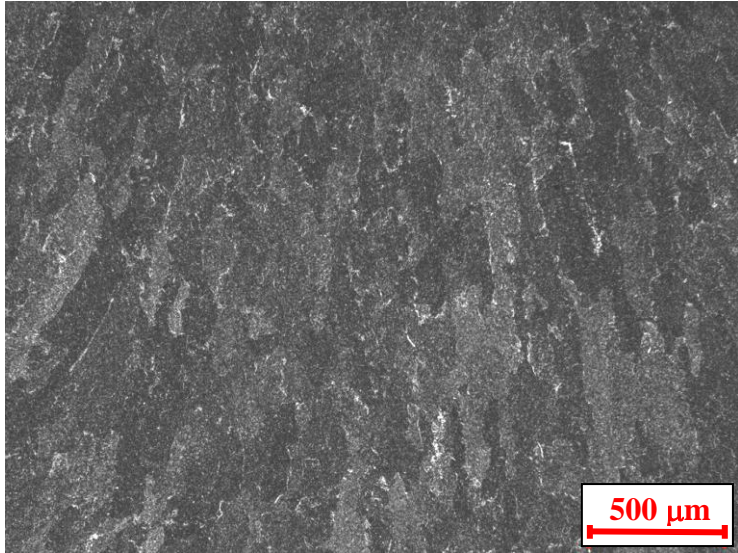
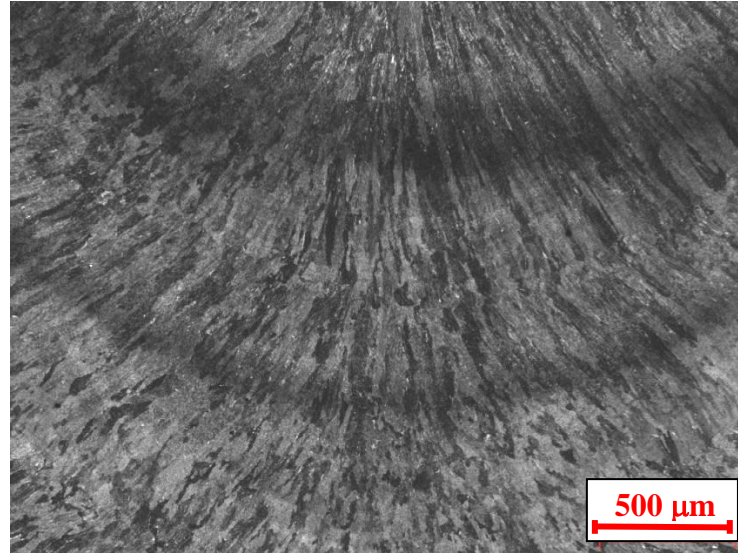


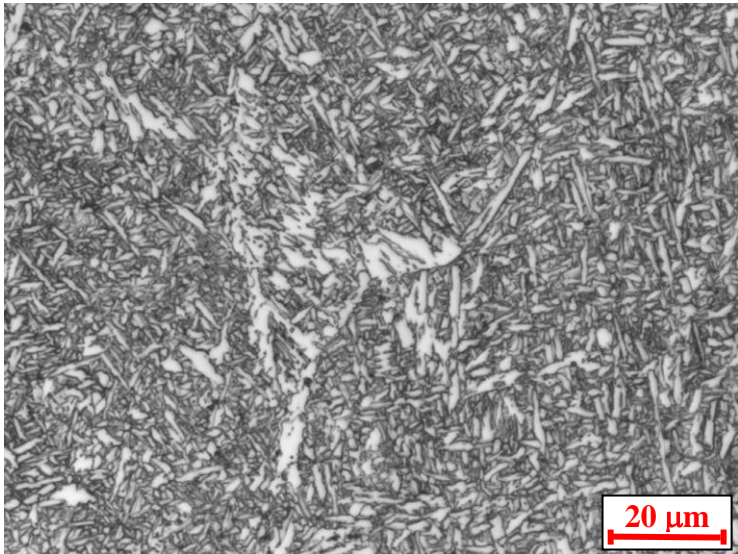
Figure 35. Microhardness maps of staggered fill passes (a) D1, (b) D2, (c) D3, (d) D4, and (e) completed weld with cap passes for dual torch X100 rolled weld 883I.



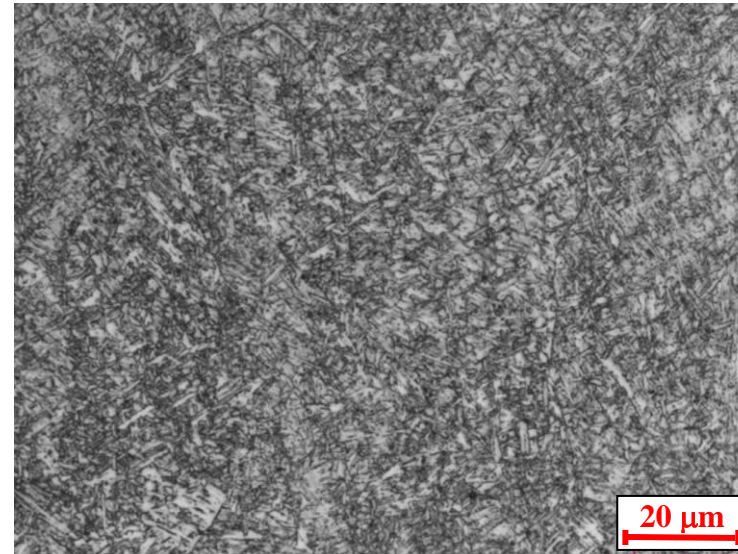
(a) NiMo80–AD WM structure for 1.5 kJ/mm region.



(c) NiMo80 –AD weld metal structure for 0.5 kJ/mm region

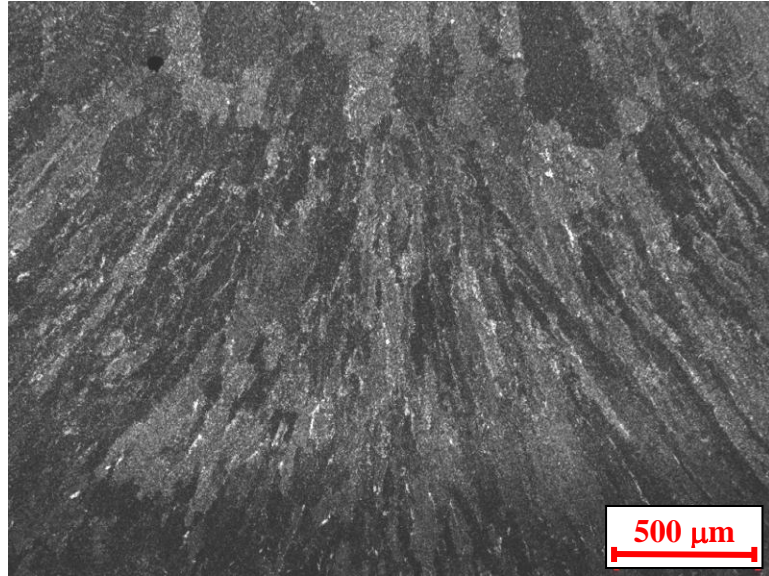


(b) NiMo80 –Detail of AD weld metal microstructure in (a)

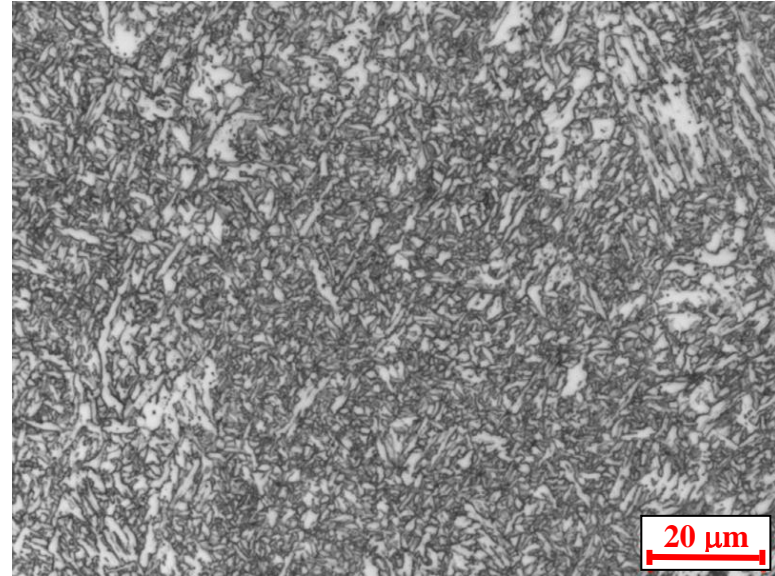


(d) NiMo80 – Detail of AD weld metal microstructure in (c)

Figure 36. Micrographs of as deposited weld metal regions in experimental plate weld NiMo80.

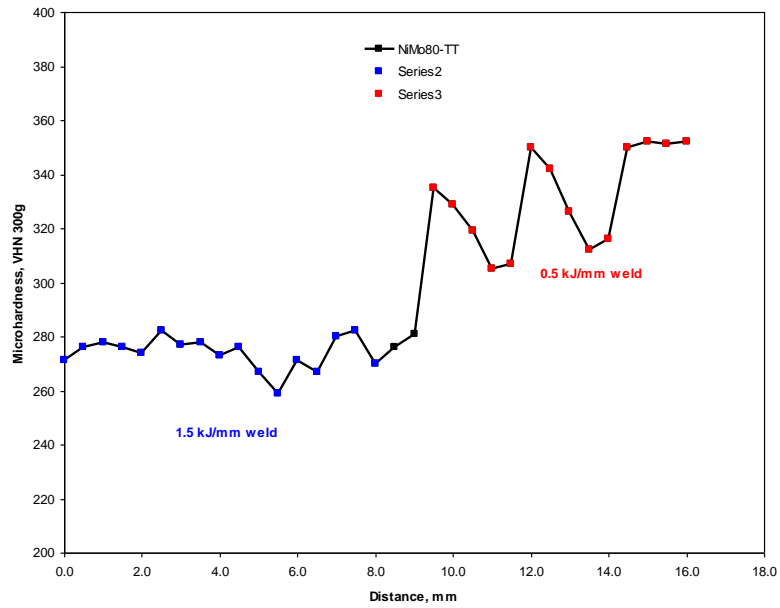


(a) Reheated structure formed under 1.5 kJ/mm weld pass

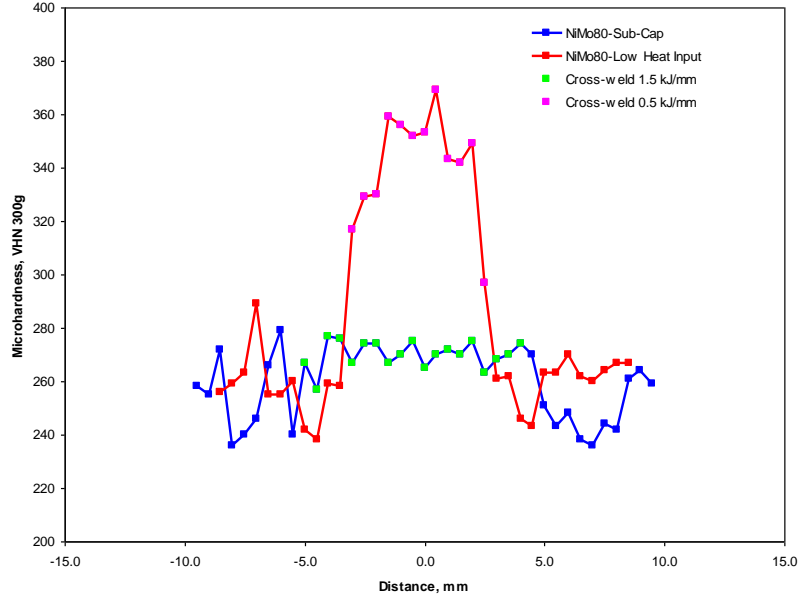


(b) Detail of reheated WM.

Figure 37. Micrographs of reheated WM in experimental plate weld NiMo80.



(a) Through-thickness weld centerline traverse



(b) Cross-weld traverses through 1.5 and 0.5 kJ/mm weld passes.

Figure 38. Microhardness results for plate weld NiMo80.

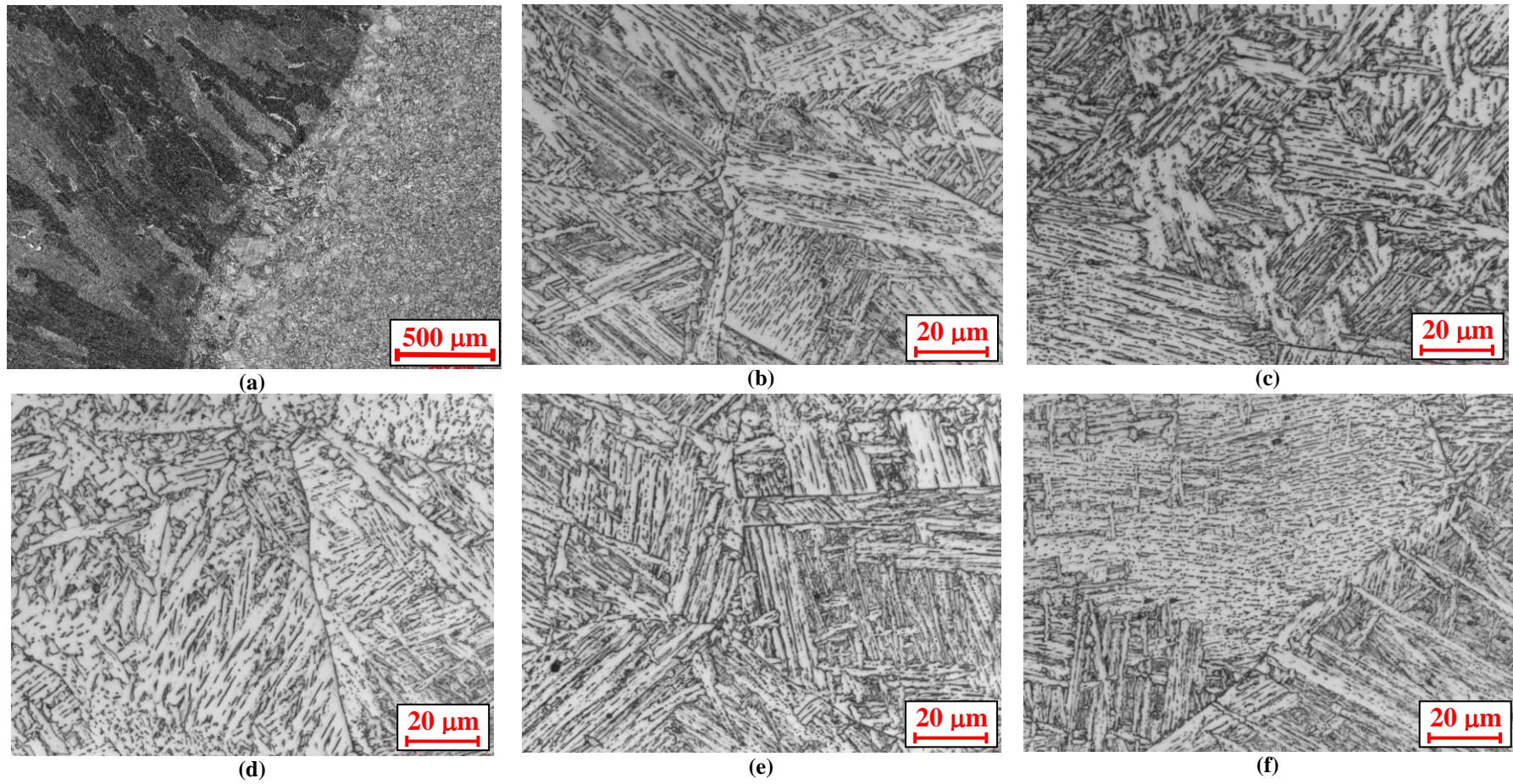


Figure 39. Optical micrographs of GCHAZ region adjacent to 1.5 kJ/mm deep-fill pass weld in X100-5 steel pipe.

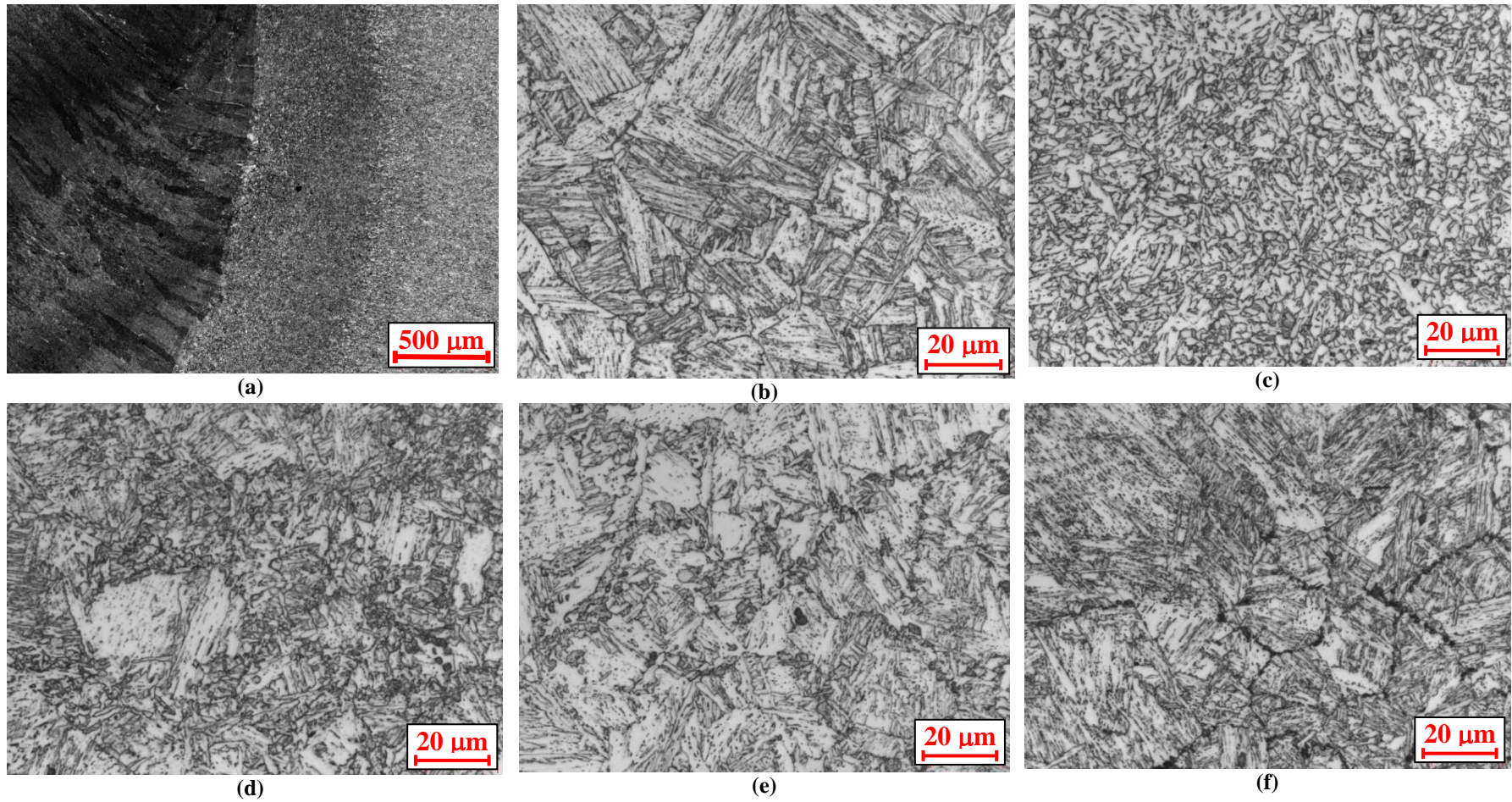


Figure 40. Optical micrographs of GHAZ regions adjacent to 0.5 kJ/mm fill passes in X100-5 steel pipe.